TTCACGCTAGTGACCG; Phlda3-R, TGGATGGCCTGTTGATTCTTGA; Gapdh-F, AACTTTGGCATTGTGGAAGG; Gapdh-R, ATGCAGGGATGATGTTCTGG. The amplified products by AmpliTaq Gold (Applied Biosystems) were separated on a 2% agarose gel and visualized with ethidium bromide. Otherwise, real-time PCR assay was carried out using Power SYBER green PCR Master kit (ABI).

Chromosome spreads

Mitotic cells were prepared by treatment with 20 ng/ml nocodazole for 6 h and then collected. The collected cells were swollen hypotonically with 75 mM KCl for 15 min, and then fixed with Carnoy's solution (75% methanol/25% acetic acid) for 20 min. After changing the fixative once, the cells were dropped in Carnoy's solution onto glass slides and air-dried. The slides were stained with 4% Giemsa (Merck) solution for 10 min, washed briefly in tap water, and air-dried.

Supporting Information

Figure S1 Representative images of MEFs during the lifespan. MEFs cultivated as in Figure 1A top lead into either immortality development under Std-3T3 or quiescence preservation under tSD-3T3. After serial cultivation, MEFs become morphologically senescent, i.e., flattened and enlarged morphology (P9) under both Std-3T3 and tSD-3T3 conditions. While continuous MEF-culture under tSD-3T3 preserved the quiescent status with continuously senescent morphology, continuous MEF-culture under Std-3T3 lead to the sporadic emergence of immortalized colony from the senescent MEFs. Immortalized MEFs (IP2) are morphologically escaped from senescence and rather similar to that in early passage (P3).
(TIF)

Figure S2 H2AX diminution is also observed in adult mice organs. Samples were prepared from five week (5W), five month (5M) and seven- or nine-month-old mice (7M or 9M). Compared to five months old organs, H2AX protein level is diminished in Testis (9M), Brain (7M), and Colon (7M), in which the diminution levels are lower than those in Liver, Spleen, and Pancreas. In Heart and Thymus, H2AX levels did not altered the alteration in through 5 weeks old to 7 or 9 months old.
(TIF)

Figure S3 H2AX diminution is also shown in damage induced premature senescence. Premature senescence was induced with NCS treatment as shown schematically in the top, in which each red arrowhead represents 100 ng/μl NCS treatment. Premature senescence by damage was induced with H2AX diminution, in which cells showed typical senescent morphology of flattened and enlarged.
(TIF)

Figure S4 H2AX transcript is decreased in quiescent MEFs. Decrease in H2AX mRNA level in senescing MEFs was observed by RT-PCR (right panel) and is compared with protein diminution (left panel).
(TIF)

Figure S5 H2AX over-expression accelerates immortality development in MEFs with tetraploidy. A. Experimental scheme of H2AX over expression. After transfection of H2AX-over expressing (H2AX-OE) or empty control vectors into early passage MEFs (P3), the transformed MEFs were selected, re-plated, and maintained in complete medium until immortalized cells appeared. **B.** Growth curves of MEFs during the experiments in A. MEFs before transfection and re-plating, MEFs transfected with H2AX-over-expressing vector, and MEFs transfected with empty control vector are indicated by black closed squares, red open circles, and black open diamonds, respectively. MEFs over-expressing H2AX showed accelerated development of immortality. **C.** H2AX status was determined as indicated in the figure. Although senescence was induced in the transfected and selected MEFs, H2AX over-expressing MEFs show higher levels of H2AX after the selection resulting in the development of immortality with H2AX recovery. **D.** Representative MEF images during accelerated immortality development with H2AX over-expression and controls. MEFs transfected with the H2AX over-expressing vector showed an efficient escape from senescence, while MEFs carrying the negative control vectors remained senescent with a flattened and enlarged morphology. **E,F.** Genomic instability status in immortalized MEFs (IP3) that were developed with H2AX over-expression was assessed by flow-cytometry (**E**) and Giemsa staining of M-phase chromosome (**F**).
(TIF)

Figure S6 p53 expression in senescing MEFs. To determine p53 expression in the cause of senescence, the expression levels of p53 and the targets (Sidt2 and Phlda3) that are likely associated with tumor suppression were compared between early passage (P2) and senescent MEFs (P7) under tSD-3T3 conditions. Along with H2AX diminution under p53 proficient background after serial cultivation, the expressions of Sidt2 and Phlda3 were observed in senescent MEFs (P7), in which the change in the expressed p53 transcript is limited.
(TIF)

Figure S7 p53 activation shown by miR34a expression in primary wt-MEFs after damage is not directly associated with H2AX expression levels at least for transcript regulation. A. To confirm p53 dependent DNA damage response, wt- and $p53^{-/-}$-MEFs in primary and immortal were treated with 200 ng/ml neocarzinostatin (NCS) for 6 hours and the expression of p53-target miR34a was assessed. As expected, miR34a expression was shown after NCS treatment in primary wt-MEFs (wild type) but neither in immortalized wt-MEFs nor in $p53^{-/-}$-MEFs. **B.** To determine the p53-activation associated change in the expression levels of H2AX transcript, mRNA levels of H2AX in MEFs treated as in **A** were analyzed. Whereas p53 is activated after NCS treatment in primary wt-MEFs, H2AX transcript levels were stable, suggesting no direct regulation by p53 transcription factor for H2AX expression. The PCR primers for miR34a were used from miRNA-specific primers (ABI) with snoRNA202 (ABI) for the control. Real-time PCR assay was carried out TaqMan microRNA assay kit (ABI).
(TIF)

Acknowledgments

We thank RIKEN BRL Cell Bank for the normal human umbilical cord fibroblast (NHF) cells (HUC-F2). We also thank K. Shimizu-Saito, M. Yanokura, and I. Kobayashi for technical support. We are grateful to S. Takeda, W. Bonner, P. Hsieh, K. Okamoto, and S. Nakada for critical reading of the manuscript and to T. Tsuzuki and Y. Nakatsu for critical discussion of the study.

Author Contributions

Conceived and designed the experiments: KY. Performed the experiments: YA H. Fuji H. Fukuda AI KS YY MS YI JU KY. Analyzed the data: H. Fuji KY. Contributed reagents/materials/analysis tools: SM NT YH HN MM. Wrote the paper: KY H. Fukuda HT.

References

1. Negrini S, Gorgoulis VG, Halazonetis TD (2010) Genomic instability–an evolving hallmark of cancer. Nat Rev Mol Cell Biol 11: 220–228.
2. Lengauer C, Kinzler KW, Vogelstein B (1997) Genetic instabilities in colorectal cancers. Nature 386: 632–627.
3. Lengauer C, Kinzler KW, Vogelstein B (1998) Genetic instabilities in human cancers. Nature 396: 643–649.
4. Stephans PJ, Greenman CD, Fu B, Yang F, Bignell GR, et al. (2011) Massive genomic rearrangement acquired in a single catastrophic event during cancer development. Cell 144: 27–40.
5. Vitale I, Galluzzi L, Senovilla L, Criollo A, Jemaà M, et al. Illicit survival of cancer cells during polyploidization and depolyploidization. Cell death differ, doi: 10.1038/cdd.2010.145.
6. Danes BS (1978) Increased in vitro tetraploidy: tissue specific within the heritable colorectal cancer syndromes with polyposis coli. Cancer 41: 2330–2334.
7. Dutrillaux B, Gerbault-Seureau M, Remvikos Y, Zafrani B, Prieur M (1991) Breast cancer genetic evolution: I. Data from cytogenetics and DNA content. Breast Cancer Res Treat 19: 245–255.
8. Heselmeyer K, Schröck E, du Manoir S, Blegen H, Shah K, et al. (1996) Gain of chromosome 3q defines the transition from severe dysplasia to invasive carcinoma of the uterine cervix. Proc Natl Acad Sci USA 93: 479–484.
9. Maley CC, Galipeau PC, Li X, Sanchez CA, Paulson TG, et al. (2004) The combination of genetic instability and clonal expansion predicts progression to esophageal adenocarcinoma. Cancer Res 64: 7629–7633.
10. Ichijima Y, Yoshioka K, Yoshioka Y, Shinohe K, Fujimori H, et al. (2010) DNA lesions induced by replication stress trigger mitotic aberration and tetraploidy development. PLoS One 5: e8821.
11. Bartkova J, Horejsí Z, Koed K, Krämer A, Tort F, et al. (2005) DNA damage response as a candidate anti-cancer barrier in early human tumorigenesis. Nature 434: 864–870.
12. Gorgoulis VG, Vassiliou LV, Karakaidos P, Zacharatos P, Kotsinas A, et al. (2005) Activation of the DNA damage checkpoint and genomic instability in human precancerous lesions. Nature 434: 907–913.
13. Sedelnikova OA, Horikawa I, Zimonjic DB, Popescu NC, Bonner WM, et al. (2004) Senescing human cells and ageing mice accumulate DNA lesions with unrepairable double-strand breaks. Nature Cell Biol 6: 168–170.
14. Nakamura AJ, Chiang YJ, Hathcock KS, Horikawa I, Sedelnikova OA, et al. (2008) Both telomeric and non-telomeric DNA damage are determinants of mammalian cellular senescence. Epigenetics Chromatin 1: 6.
15. Geigl JB, Langer S, Barwisch S, Pfleghaar K, Lederer G, et al. (2004) Analysis of gene expression patterns and chromosomal changes associated with aging. Cancer Res 64: 8550–8557.
16. Sherr CJ, Weber JD (2000) The ARF/p53 pathway. Curr Opin Genet Dev 10: 94–99.
17. Sherr CJ (1998) Tumor surveillance via the ARF-p53 pathway. Genes Dev 12: 2984–2991.
18. Matheu A, Maraver A, Serrano M (2008) The Arf/p53 pathway in cancer and aging. Cancer Res 68: 6031–6034.
19. Tyner SD, Venkatachalam S, Choi J, Jones S, Ghebranious N, et al. (2002) p53 mutant mice that display early ageing-associated phenotypes. Nature 415: 45–53.
20. Maier B, Gluba W, Bernier B, Turner T, Mohammad K, et al. (2004) Modulation of mammalian life span by the short isoform of p53. Genes Dev 18: 306–319.
21. Varela I, Cadiñanos J, Pendás AM, Gutiérrez-Fernández A, Folgueras AR, et al. (2005) Accelerated ageing in mic deficient in Zmpste24 protease is linked to p53 signalling activation. Nature 437: 564–568.
22. Matheu A, Maraver A, Klatt P, Flores I, Garcia-Cao I, et al. (2007) Delayed ageing through damage protection by the Arf/p53 pathway. Nature 448: 375–379.
23. Parrinello S, Samper E, Krtolica A, Goldstein J, Melov S, et al. (2003) Oxygen sensitivity severely limits the replicative lifespan of murine fibroblasts. Nature Cell Biol 5: 741–746.
24. Bassing CH, Chua KF, Sekiguchi J, Suh H, Whitlow SR, et al. (2002) Increased ionizing radiation sensitivity and genomic instability in the absence of histone H2AX. Proc Natl Acad Sci USA 99: 8173–8178.
25. Celeste A, Petersen S, Romanienko PJ, Fernandez-Capetillo O, Chen HT, et al. (2002) Genomic instability in mice lacking histone H2AX. Science 296: 922–927.
26. Bronson R, Lee C, Alt WF (2003) Histone H2AX: A dosage-dependent suppressor of oncogenic translocations and tumors. Cell 114: 359–370.
27. Bassing CH, Alt FW (2004) H2AX May Function as an Anchor to Hold Broken Chromosomal DNA Ends in Close Proximity. Cell Cycle 3: 149–153.
28. Bonner WM, Redon CE, Dickey JS, Nakamura AJ, Sedelnikova OA, et al. (2008) GammaH2AX and cancer. Nature Rev Cancer 8: 957–967.
29. Tsukuda T, Fleming AB, Nickoloff JA, Osley MA (2005) Chromatin remodelling at a DNA double-strand break site in Saccharomyces cerevisiae. Nature 438: 379–383.
30. Keogh MC, Mennella TA, Sawa C, Berthelet S, Krogan NJ, et al. (2006) The Saccharomyces cerevisiae histone H2A variant Htz1 is acetylated by NuA4. Genes Dev 20: 660–665.
31. Ikura T, Tashiro S, Kakino A, Shima H, Jacob N, et al. (2007) DNA damage-dependent acetylation and ubiquitination of H2AX enhances chromatin dynamics. Mol Cell Biol 27: 7028–7040.
32. Brady CA, Jiang D, Mello SS, Johnson TM, Jarvis LA, et al. (2011) Distinct p53 transcriptional programs dictate acute DNA-damage responses and tumor suppression. Cell 145: 571–583.
33. Ceribelli M, Alcalay M, Viganò MA, Mantovani R (2006) Repression of new p53 targets revealed by ChIP on chip experiments. Cell Cycle 5: 1102–1110.
34. Yoshioka K, Yoshioka Y, Hsieh P (2006) ATR kinase activation mediated by MutSα and MutLα in response to cytotoxic O6-methylguanine adducts. Mol Cell 22: 501–510.
35. Tatemichi M, Tazawa H, Masuda M, Saleem M, Wada S, et al. (2004) Suppression of thymic lymphomas and increased nonthymic lymphomagenesis in Trp53-deficient mice lacking inducible nitric oxide synthase gene. Int J Cancer 111: 819–828.
36. Todaro GJ, Green H (1963) Quantitative studies of the growth of mouse embryo cells in culture and their development into established lines. J Cell Biol 17: 299–313.
37. Lukas C, Melander F, Stucki M, Falck J, Bekker-Jensen S, et al. (2004) Mdc1 couples DNA double-strand break recognition by Nbs1 with its H2AX-dependent chromatin retention. EMBO J 23: 2674–2683.
38. Dimitrova N, de Lange T (2006) MDC1 accelerates nonhomologous end-joining of dysfunctional telomeres. Genes Dev 20: 3238–3243.

OPEN ACCESS Freely available online

PLoS one

DNA Lesions Induced by Replication Stress Trigger Mitotic Aberration and Tetraploidy Development

Yosuke Ichijima[1], Ken-ichi Yoshioka[1,2]*, Yoshiko Yoshioka[1], Keitaro Shinohe[1], Hiroaki Fujimori[1,2], Junya Unno[3], Masatoshi Takagi[3], Hidemasa Goto[4], Masaki Inagaki[4], Shuki Mizutani[3], Hirobumi Teraoka[1]

1 Department of Pathological Biochemistry, Medical Research Institute, Tokyo Medical and Dental University, Tokyo, Japan, 2 Biochemistry Division, National Cancer Center Research Institute, Tokyo, Japan, 3 Department of Pediatrics and Developmental Biology, Tokyo Medical and Dental University Graduate School, Tokyo, Japan, 4 Division of Biochemistry, Aichi Cancer Center Research Institute, Nagoya, Japan

Abstract

During tumorigenesis, cells acquire immortality in association with the development of genomic instability. However, it is still elusive how genomic instability spontaneously generates during the process of tumorigenesis. Here, we show that precancerous DNA lesions induced by oncogene acceleration, which induce situations identical to the initial stages of cancer development, trigger tetraploidy/aneuploidy generation in association with mitotic aberration. Although oncogene acceleration primarily induces DNA replication stress and the resulting lesions in the S phase, these lesions are carried over into the M phase and cause cytokinesis failure and genomic instability. Unlike directly induced DNA double-strand breaks, DNA replication stress-associated lesions are cryptogenic and pass through cell-cycle checkpoints due to limited and ineffective activation of checkpoint factors. Furthermore, since damaged M-phase cells still progress in mitotic steps, these cells result in chromosomal mis-segregation, cytokinesis failure and the resulting tetraploidy generation. Thus, our results reveal a process of genomic instability generation triggered by precancerous DNA replication stress.

Citation: Ichijima Y, Yoshioka K-i, Yoshioka Y, Shinohe K, Fujimori H, et al. (2010) DNA Lesions Induced by Replication Stress Trigger Mitotic Aberration and Tetraploidy Development. PLoS ONE 5(1): e8821. doi:10.1371/journal.pone.0008821

Editor: Mikhail V. Blagosklonny, Roswell Park Cancer Institute, United States of America

Received October 8, 2009; **Accepted** December 18, 2009; **Published** January 21, 2010

Funding: This study was supported by the Ministry of Education, Culture, Sports, Science and Technology (MEXT) KAKENHI (20770136, 20659047). The funders had no role in study design, cata collection and analysis, decision to publish, or preparation of the manuscript.

Competing Interests: The authors have declared that no competing interests exist.

* E-mail: kyoshiok@ncc.go.jp

Introduction

Genomic instability is observed in most cancer cells [1]. In the earliest stages of cancer development, cells exhibit DNA lesions, which are characterized as precancerous DNA lesions and are induced by DNA replication stress with the accelerated cell cycle progression as the results of oncogene acceleration or of aberrant growth activation [2,3]. During these stages, although anti-cancer barrier reactions including cell cycle arrest and inductions of senescence and apoptosis are also competitively activated to block the tumorigenesis step progression [2,3], genomic instability is subsequently started to appear prior to the development of cancer [2,3]. However, the process by which precancerous lesions cause genomic instability remains unclear.

The most common types of genomic instability in cancer cells are alterations in the number of chromosomes, i.e., aneuploidy [4]. Aneuploidy is suggested to develop via unstable intermediates of tetraploidy [5,6]. In addition, tetraploidy even contributes to tumourigenesity *in vivo* [7]. Therefore, the process to generate tetraploidy must be a critical step for the development of many cancers. Furthermore, consistent with the hypothesis of aneuploidy development via unstable tetraploidy intermediates, cancer cells with chromosomal instability show the characteristics of continuous alteration in chromosomal status, highlighting the question for the initiation and the induction of tetraploidy.

Although it is elusive how tetraploidy is developed during cellular transformation, tetraploidy is often observed in cells lacking in the M-phase function [8], which also promotes tumourigenesis [9,10]. Spontaneous tetraploidization is also observed in association with chromosome bridges during mitotic chromosome segregation and the resulting cytokinesis failure [11]. Since the appearance of precancerous lesions is followed by the development of genomic instability [2,3], we hypothesized here that, prior to cellular transformation, precancerous DNA lesions are carried over into the M phase, causing mitotic aberrations, including chromosome-bridge formation to lead into tetraploidy generation, contributing cancer development (Supplementary Fig. S1).

For the above hypothesis, we investigated effects of DNA replication stress-associated lesions by oncogene acceleration or by hydroxyurea treatment as well as impacts of DNA lesions in the M phase, and also studied the immortalization process of primary mouse embryonic fibroblasts (MEFs). Here, we found that DNA replication stress-associated lesions can be transmitted into the M phase, unlike directly induced DNA double-strand breaks, resulting in successive chromosomal mis-segregation, cytokinesis failure and tetraploidy generation. Importantly, we observed that these happen during cellular immortalization, and found that senescing cells are temporarily accumulated with bi-nuclear tetraploidy, which is a form right after the tetraploidy generation, prior to the acquirement of the immortality.

Results

DNA Lesions Induced by Oncogenes Accumulate in the M Phase

To test the above hypothesis (Supplementary Fig. S1), we initiated a study of DNA lesions induced by oncogenes, such as *E2F1*, because the initial stages of cancer development are mimicked by oncogene-acceleration, in which genomic instability is subsequently developed [2]. To determine the effects of the accelerated oncogene function, the spontaneous accumulation of M-phase DNA lesions was monitored with a double staining of γH2AX, a DNA-damage marker, and histone H3 phosphorylated at Ser 10 (p-H3), an M-phase marker (Fig. 1). *E2F1* acceleration caused DNA lesions in U2OS cells (Fig. 1A, B), mimicking the initial stages of cancer development as previously reported [2]. In addition, we observed that these induced DNA lesions are accumulated in mitotic cells (Fig. 1A, C). Similar results were also observed by using another oncogene *Cdc25A* in HEK293 cells (Fig. 1D, E; Supplementary Fig. S2). Thus, supporting our hypothesis (Supplementary Fig. S1), these results show that oncogenic DNA lesions are also appeared in the M phase and indicate the close correlation between mitotic precancerous DNA lesions and genomic instability development.

Oncogene Acceleration Induces Chromosome-Bridge and Aneuploidy

To explore the possible correlation between mitotic DNA lesions and the induction of genomic instability, we determined the appearance of chromosome bridges, because a recent study has shown that spontaneous tetraploidization is triggered by chromosome bridges [11], though it remains elusive how chromosome bridges are induced. After *E2F1* acceleration, we observed chromosome bridges (Fig. 2A) concomitantly with the elevation of polyploidy fraction (Fig. 2B). Intriguingly, such a chromosome bridge was observed with γH2AX signal on the chromosome (Fig. 2A), indicating the involvement of DNA lesions in the

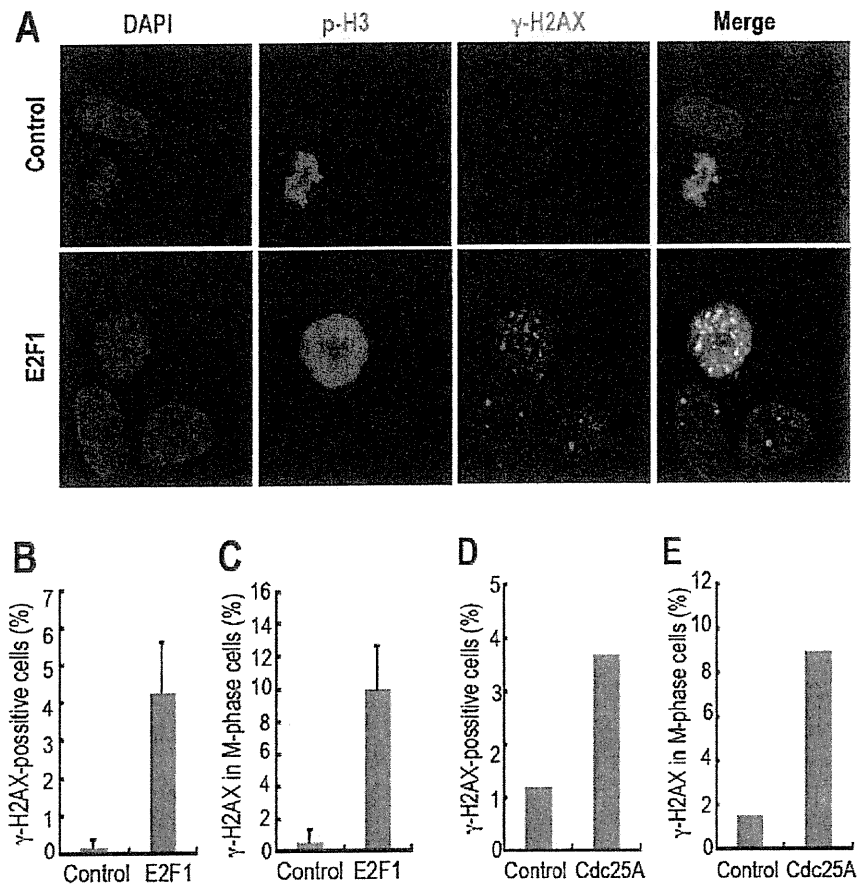

Figure 1. DNA lesions induced by oncogene acceleration are accumulated in the M phase. A. DNA lesions in the M phase were determined by a double staining of γH2AX and p-H3 after nocodazole treatment (100 ng/ml, 12 h). Using ER-*E2F1*-expressing U2OS cells, DNA lesion-carryover into the M phase was evaluated after treatment with 4-hydroxytamoxifen for 6 h (E2F1). Representative images are shown before (control) and after E2F1 activation (E2F1). **B,C.** The proportions of total γH2AX-positive cells (**B**) and γH2AX/p-H3 double-positive cells (**C**) were estimated in the cells prepared as in **A**. At least 50 cells were counted in each of 3 independent experiments. Error bars represent ± SD. **D,E.** Transient over-expression of *Cdc25A* promotes DNA lesions including the cells during mitosis. The proportions of total γH2AX-positive cells (**D**) and γH2AX/p-H3 double-positive cells (**E**) were estimated by counting at least 60 cells in **D** and 500 cells in **E**. Representative fluorescent microscope images are also shown in supplementary Fig. S2.
doi:10.1371/journal.pone.0008821.g001

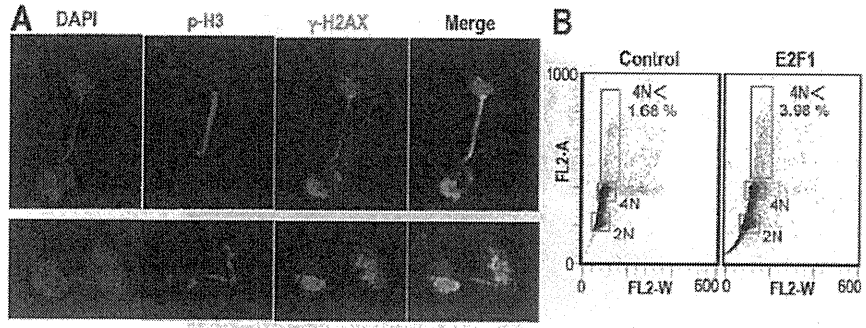

Figure 2. E2F1 acceleration generates chromosome bridge and aneuploidy. A. After E2F1 activation as in Figure 1A, chromosome bridges were often observed with the generated DNA lesions by E2F1 activation. Representative images are shown. B. Cells containing more than 4N DNA content were detected by flow cytometry in the cells treated as in Figure 1A. The proportions of cells with DNA content of 2N, 4N and more (4N<) are indicated by red squares. The percentages of 4N< cells are indicated. The sub-G1 fraction was also observed in E2F1-activated cells.
doi:10.1371/journal.pone.0008821.g002

chromosome bridge formation. Taken together, these results support our hypothesis (Supplementary Fig. S1) and indicate that precancerous DNA lesions induced by oncogenes trigger chromosome bridges during mitosis and induce genomic instability. However, oncogene activation primarily accelerates S-phase entry, thereby the resulting DNA lesions are primarily associated with DNA replication stress in the S phase [2]. Here, an important question arose, if the observed M-phase lesions possibly transmit into the M phase from the S phase with the bypass of cell cycle checkpoints.

DNA Replication Stress-Associated Lesions Transmit into the M Phase

To directly determine the potential of DNA lesion-carryover generated by DNA replication stress in the S phase, we transiently treated the normal human fibroblast SuSa with hydroxyurea (HU) to cause replication fork stalling and the resulting DNA double-strand breaks. After the transient replication stress, γH2AX foci were evidently increased in the subsequent M phase (Fig. 3A,B), showing that DNA lesions induced by replication stress actually transmit into the M phase. However, an important question remains: How can DNA lesions generated by replication stress be carried over into the M phase, despite the existence of the firmly established intra-S and G2/M checkpoints?

Recently, DNA lesion-carryover into the M phase has been shown with fewer than 20 foci of γH2AX per nucleus in the ATM-mutated background after X-ray or γ-ray irradiation [12], implying that cell cycle checkpoints are bypassed under a small number of lesions with compromised damage checkpoint response. To determine the status of DNA lesions and checkpoint activation, we compared γH2AX signals and phosphorylated ATM (p-ATM) signals after *E2F1* acceleration with those of the radiomimetic agent neocarzinostatin (NCS) that causes G2-arrest. While NCS causes γH2AX and the resulting p-ATM foci in the entire nucleus, *E2F1* acceleration was found to cause only very limited γH2AX (Fig. 4A) and the resulting much weaker and limited p-ATM foci (Fig. 4B), indicating only local checkpoint activation. Taken together, our results suggest that DNA lesions induced by replication stress under *E2F1* acceleration, unlike directly induced DNA double-strand breaks, impact a small number of DNA lesions, resulting in limited damage checkpoint response, bypass of cell-cycle checkpoints and DNA lesion-carryover into the M phase.

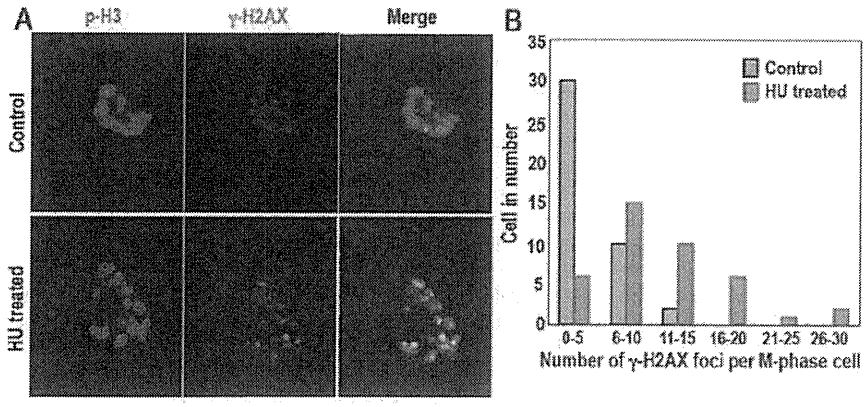

Figure 3. DNA lesions induced by replication stress are transmitted into the M phase. A,B. Using the normal human fibroblast SuSa, the carryover of DNA replication stress-associated lesions was determined after the transient treatment of 1 mM HU for 24 h and the subsequent nocodazole block as in Methods. The representative images (**A**) and the number of γH2AX foci per cell (**B**) are shown. The number of γH2AX foci was counted from 42 control cells and 40 replication stress-induced cells.
doi:10.1371/journal.pone.0008821.g003

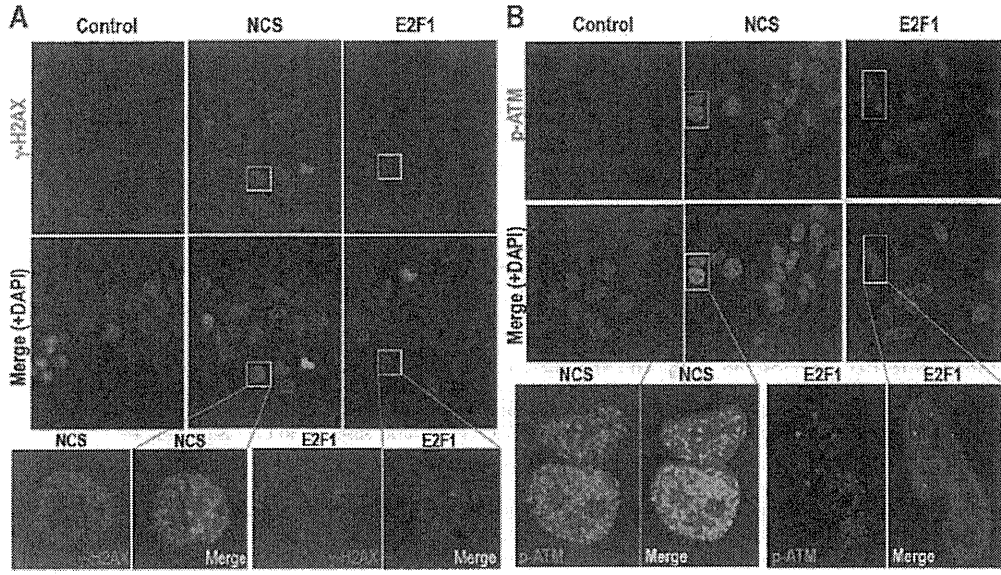

Figure 4. DNA replication stress causes only a small number of DNA lesions with limited ATM activation. A,B. Comparing cells activated with E2F1 as in Fig. 1A and cells damaged with 100 ng/ml NCS that causes G2-phase arrest, the statuses of DNA lesions and the resulting damage checkpoint activation were determined with γH2AX foci (**A**) and phosphorylated ATM (P-ATM) foci (**B**), respectively.
doi:10.1371/journal.pone.0008821.g004

DNA Lesions in the M Phase Cause Cytokinesis Failure

Another question remains: How do mitotic cells readily respond to DNA lesions that are carried over into the M phase? Despite the numerous studies on DNA damage response, only a few studies of those have been reported for the mitotic cells, showing M-phase specific DNA damage checkpoints [13,14]. Interestingly, one of these has reported tetraploidization with ionizing radiation in prometaphase HeLa cells [13]. Here, we found that such tetraploidization is a common phenomenon, independent of damaging sources (Fig. 5A) and cell types, including U2OS, WI-38, and MEFs (Supplementary Fig. S3), as long as cells existed in the M phase (Supplementary Fig. S4). These showed completely different responses to DNA damage in the M phase.

For the detailed study on tetraploidization with DNA lesions in mitotic cells, we used time-lapse imaging (Fig. 5B; Supplementary Movies S1, S2, S3, S4) and found that the damaged cells failed to complete cytokinesis and subsequently developed tetraploidy (Fig. 5B lower panels between 4:30 and 5:00). Importantly, such a cytokinesis failure was observed in the majority of cells (Supplementary Movie S4; Fig. 5A), and those still replicated DNA (Supplementary Fig. S5). Furthermore, despite the activation of DNA damage checkpoint proteins, including H2AX, ATM and Chk2 (Fig. 5C; Supplementary Fig. S6), damaged M-phase cells still exited from the mitotic phase and entered into the G1 phase, based on monitoring cyclins B and E as M- and G1-phase markers, respectively (Fig. 5D), indicating the dysfunctional DNA damage checkpoint during mitosis. Since cells had already exited from the metaphase, the spindle assembly checkpoint could not be responsible for DNA damage. In fact, a spindle assembly checkpoint factor, BubR1, exhibited normally (Supplementary Fig. S7). Thus, DNA damage checkpoints are not fully functional during mitosis, even if they exist [13,14].

In addition, tetraploidization was also observed in metaphase cells but was significantly lowered 15 min after metaphase release (Fig. 6A), suggesting the involvement of chromosome segregation, because chromosome segregation starts at the onset of the anaphase. In fact, the cells damaged in the prometaphase showed incomplete chromosome segregation (Fig. 6B). Furthermore, such chromosomal mis-segregation disrupted the spindle midzone structure, including Aurora-B localization (Fig. 6C), which is the essential conformation for cytokinesis [15,16]. Here, Aurora-B kinase was still active (Fig. 6D), though. A recent study has shown that Aurora-B functions to protect tetraploidization as an abscission checkpoint, although this is not the perfect block, either [11]. Taken together, these findings indicate that DNA lesions in the M phase cause a chromosome bridge and disrupt the spindle midzone structure, risking cytokinesis failure and tetraploidization.

MEFs Are Immortalized with Tetraploidy

As described above, DNA lesions induced by oncogenes, which could act as precancerous DNA lesions, are possibly carried over into the M phase, causing a chromosome-bridge and the resulting cytokinesis failure with tetraploidy generation. To confirm whether such scenario is really the case during spontaneous cell immortalization, we tested during the process of MEF-immortalization, (1) because MEFs are immortalized with the mutation in the Arf/p53 module similar to cancer development [17], (2) because primary MEFs often develop tetraploidy prior to immortalization, and (3) because senescing cells are known to spontaneously accumulate unrepairable DNA lesions [18], as potentially precancerous DNA lesions. We cultured growing-MEFs under the 3T3 protocol [19] and maintained senescing-MEFs with medium change (Fig. 7A). As well established, MEFs initially showed primary growth and then slowed down during senescene, which was followed by development of immortality. Intriguingly, all immortalized MEFs at early steps (IP2) were completely tetraploidy (Fig. 7B), implying that tetraploidization is the key step for MEF-immortalization. In addition, these immortalized MEFs lost the function of p53 accumulation in response to DNA damage, whereas senescing MEFs as well as

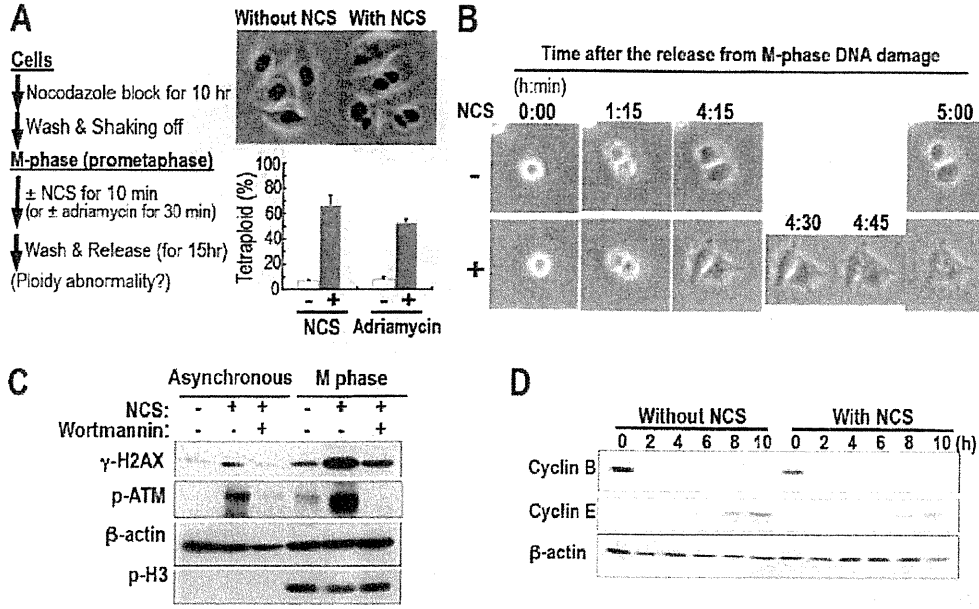

Figure 5. Damaged mitotic cells still proceed into cytokinesis with failure, resulting in tetraploidy generation. A. The tetraploidy generation was determined as in the scheme with DNA damage in the M phase. The fraction of tetraploidy was quantified from at least 100 cells in each of 3 independent experiments. Error bars in the graphs represent ± SD. **B.** Time-lapse imaging analyses were performed for the damaged cells as in **A** after the release. The representative images are displayed at the indicated time points. These results are also shown with movies [Supplementary movies S1, S3 (control) and S2, S4 (damaged with NCS)]. **C.** Mitotic cells still show the functional activation of DNA damage checkpoint factors, although cells still proceed into the G1 phase as in **D**. When indicated, the cells were incubated with 40 μM wortmannin for 1 h before NCS treatment. **D.** M-phase exit and G1-phase entry of the damaged cells as in **A** were determined with cyclins B and E as M- and G1-phase markers, respectively, after the release.
doi:10.1371/journal.pone.0008821.g005

primary growing MEFs showed p53 accumulation after DNA damage (Supplementary Fig. S8). This suggests that the induction of mutations is also associated with genomic instability development during immortality acquirement, although it is still unclear how the mutations are induced.

Spontaneous MEF-Tetraploidization Is Associated with M-Phase DNA Lesions and Chromosome-Bridge

To determine the possible association between M-phase DNA lesions and tetraploidy generation during MEF-imortalization, we examined the status of DNA lesions in the M-phase cells in each stage during the lifecycle of MEFs (Fig. 7C). Importantly, DNA-lesions in the mitotic cells were observed in the rarely growing senescent (M4 and M6) as well as in immortalized MEFs (IP32), but not in MEFs under primary growth (P4) or early senescence (M2) (Fig. 7C). These results indicate that spontaneous DNA lesions in the M phase starts to appear in the rarely growing senescent MEFs prior to the acquirement of immortality. Importantly, M-phase DNA lesions at M4 concurrently appeared with chromosome-bridge (Fig. 7D) and bi-nuclear tetraploidy (Fig. 7E). These results support that DNA lesions trigger the chromosome-bridge and the resulting tetraploidy generation during MEF-immortalization, because the observed bi-nuclear tetraploidy is a primary and transient status right after the development until the following M phase, in which daughter chromosomes assemble in a common metaphase plate to lead into tetraploidy with a single nucleus in the subsequent G1 phase [11]. Importantly, these results indicate that tetraploidy-generation associated with mitotic DNA-lesions is also the case during MEF immortalization. Furthermore, the resulting immortal MEFs (IP2) were totally tetraploidy (Fig. 7B), indicating that the tetraploidization step is critical for acquiring immortality. In addition, DNA lesions spontaneously accumulating in senescing cells act qualitatively similar to the lesions induced by oncogenes.

After immortalization, MEFs were mostly γH2AX-positive and continuously showed DNA lesions during mitosis (Fig. 7C), suggesting continuous genomic alterations. In fact, the continuous culture of immortalized MEFs resulted in chromosomal loss, i.e., aneuploidy, at IP32 (Fig. 7B), which is an identical characteristic to cancer cells showing continuous chromosomal instability [1]. These results also support the previously proposed hypothesis, i.e., aneuploidy generation via the unstable tetraploidy [5,6]. However, these M-phase lesions in the immortalized MEFs did not trigger further polyploidy generation (Fig. 7B). Similarly, tetraploidy causes growth retardation and thereby never becomes major, although spontaneous development of tetraploidy is often observed during HeLa cell cultivation via chromosome bridges [11]. While tetraploidization with M phase-DNA lesion must be a key step for acquiring immortality, the impact of tetraploidization is likely to different once cells are immortalized. Nevertheless, our results suggest that, during senescing MEF immortalization, M phase-DNA lesions trigger spontaneous development of tetraploidy.

Tetraploidy Development in MEFs Is Accelerated by DNA Replication Stress

Through above study, we showed that DNA replication stress-associated lesions are transmitted into the M phase, that DNA lesions during mitosis cause tetraploidy generation, and that the

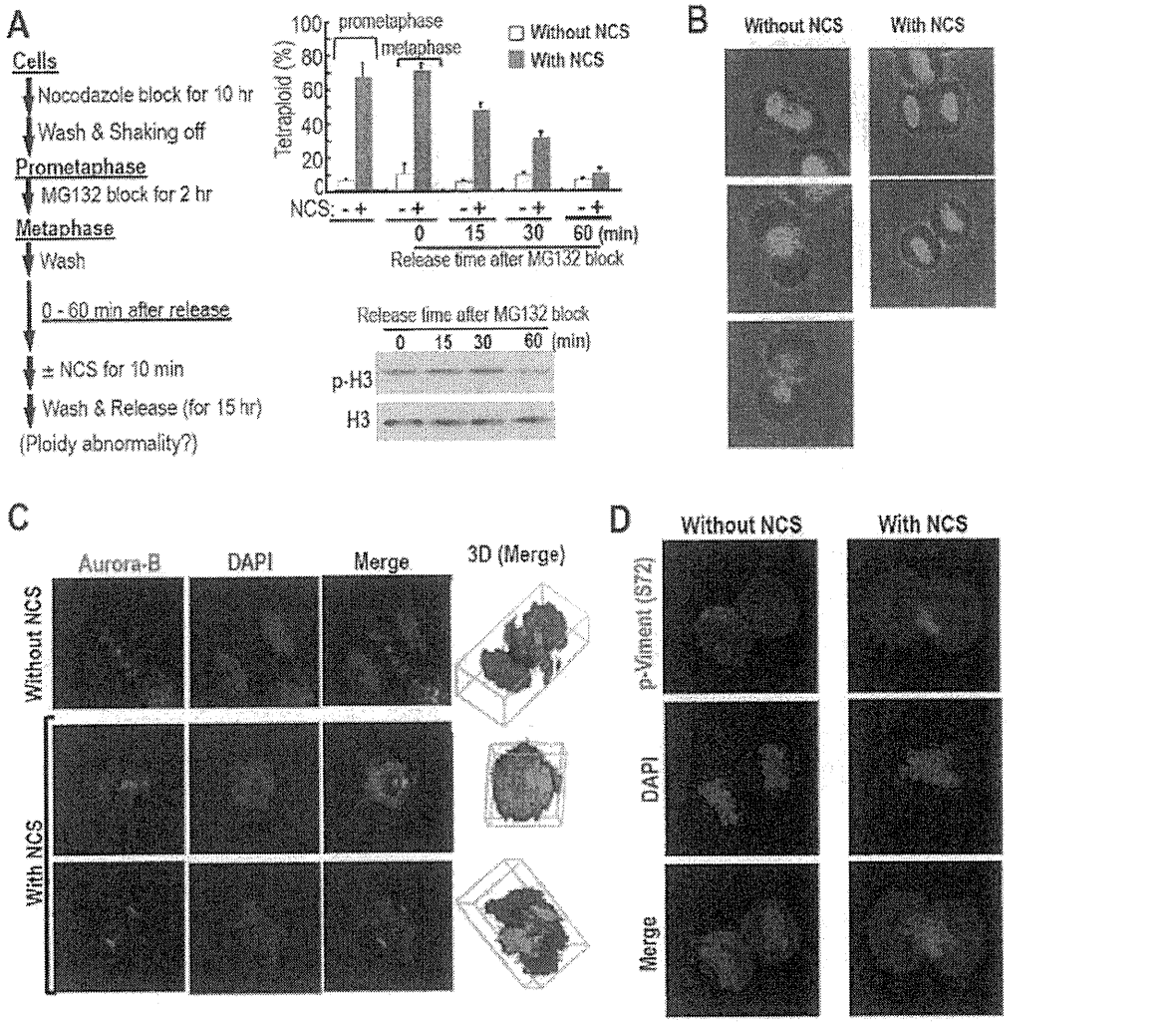

Figure 6. Mitotic DNA lesions cause chromosomal mis-segregation and a disruptive spindle mid-zone, followed by tetraploidy generation. A. DNA damage causes tetraploidy generation during metaphase but not after the onset of anaphase. The binuclear tetraploidy generation was assessed for the cells in metaphase or later as in the scheme using prometaphase cells prepared as in Figure 5A. Data were determined as in Figure 5A with at least 60 cells in each. **B.** To determine the chromosomal mis-segregation, cells damaged as in Figure 5A were released for 1 h and stained with DAPI. Images of the cells are at different mitotic stages. **C.** To determine the status of spindle midzone structure, cells damaged as in **A** were released for 1.5 h and analyzed for Aurora-B localization. Three-dimensional images are also displayed. **D.** Vimentin, a target of Aurola B, is activated with the phosphorylation status of vimentin at Ser 72 even under the chromosome mis-segregation, in which cells were treated with NCS for 1.5 h.
doi:10.1371/journal.pone.0008821.g006

identical processes are observed during the immortalization of MEFs. To directly confirm our original hypothesis (Supplementary Fig. S1), we further investigated whether tetraploidy generation could be directly induced by DNA replication stress in the pre-immortalizing MEFs (P3). Consistent with our above results, transient replication stress induced chromosome-bridge formation (Fig. 8A) and bi-nuclear tetraploidy accumulation (Fig. 8B,C) even in early passage MEFs (passage 3). Furthermore, these bi-nuclear tetraploidy MEFs were also subsequently immortalized. These indicate that DNA lesions induced by replication stress mediate tetraploidy generation in association with chromosome bridge formation during the acquirement of immortality.

Discussion

Cancer is a disease associated with genomic instability, which develops prior to tumor formation. Cells in the initial stages of cancer development exhibit precancerous DNA lesions and the competitive barrier responses [2,3]. Such stages are followed by the development of genomic instability [2,3], although it was elusive how and why genomic instability could develop in such situation. Our results showed one of the processes in developing genomic instability by precancerous DNA lesions, in which the lesions are carried over into the M phase and cause chromosomal mis-segregation and cytokinesis failure, resulting in tetraploidy generation. Such a conclusion is based on the following

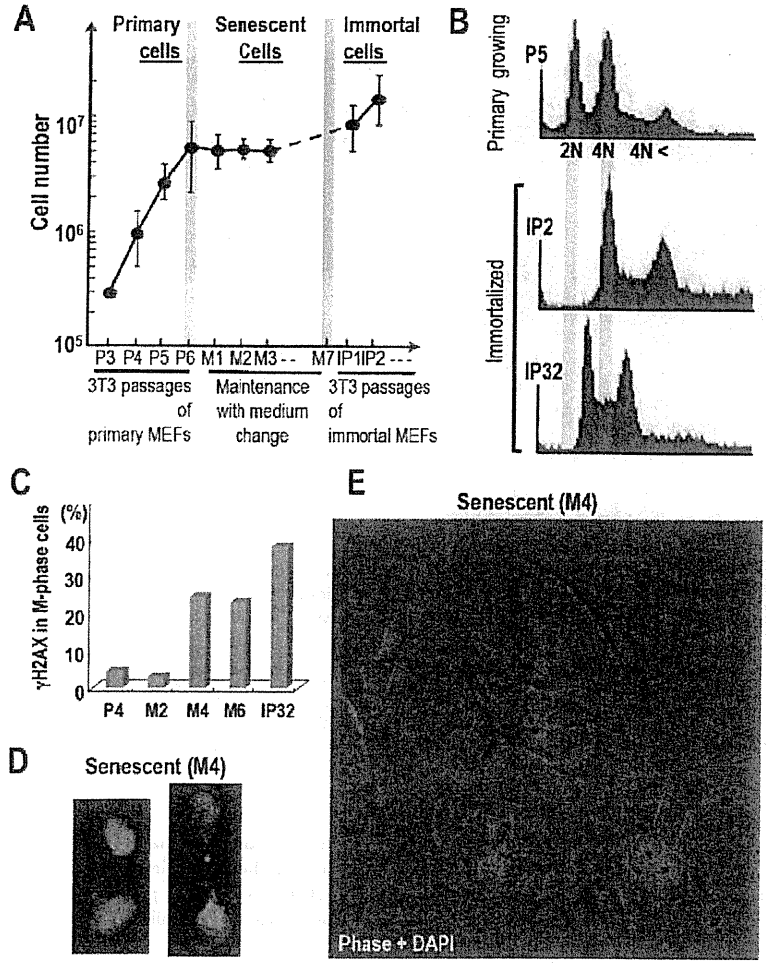

Figure 7. Senescing MEFs develop tetraploidy in association with mitotic DNA lesions and are accumulated with tetraploidy status before acquiring immortality. A. Growth curve of MEFs showed following 3 phases: primary growth (P3-P6); senescence (M1-M7); immortal growth (IP1-) phases. MEFs were passed under the 3T3 protocol or maintained with medium change once in 3 days. **B.** To determine the chromosomal status, either diploid or tetraploid/aneuploid, the chromosome contents were analyzed for primary growing (P5) and early (IP2) and late (IP32) immortalized MEFs. **C.** To determine the status of mitotic DNA lesions during the MEFs life cycle, MEFs in each step were determined by a double staining of γH2AX and phoshorylated H3 (p-H3) after nocodazole treatment (100 ng/ml, 12 h). γH2AX/p-H3 double positive fractions were determined at the indicated stages. **D.** Chromosome bridges were observed at M4. Images are representative. **E.** The image is representative at M4, showing the accumulation of cells with bi-nuclear tetraploidy. Arrowheads indicate cells with bi-nuclear tetraploid (Red arrowheads).
doi:10.1371/journal.pone.0008821.g007

mechanistic findings: DNA replication stress-associated lesions, which are induced by oncogene acceleration, can be carried over into the M phase; DNA lesions in mitotic cells cause chromosomal mis-segregation and the resulting cytokinesis failure.

Genomic instability is categorized in chromosomal instability (CIN) and microsatellite instability (MIN) [4]. While MIN is mostly characterized by mismatch repair (MMR) deficiency, CIN is usually MMR proficient. Our study revealed a process of CIN generation, especially tetraploidy/aneuploidy. Similarly, a previous study has shown that chromosomal translocation is also observed with G2-phase DNA lesions in the following G1 phase [20]. Thus, aberrant chromosomal segregation induced by DNA lesions might generally cause chromosomal alteration with the resulting loss of genomic homeostasis, which is also consistent with the observation of chromosomal loss in association with M-phase DNA lesions during the continuous culture of the immortalized MEFs (Fig. 7B).

Consistent with ageing-associated cancer-risk elevation, our results suggest that spontaneous DNA lesions accumulated in senescent cells during MEF immortalization act as precancerous DNA lesions, similar to the lesions induced by oncogene acceleration. Our results also show that DNA lesions generated by DNA replications stress are cryptogenic due to the limited impact on DNA lesions and the checkpoint activation, and that these lesions therefore induce genomic instability after the transmission into the M phase. Such a conclusion, i.e., genomic instability induction by DNA replication stress, is supported by the evidence of cancer predisposition with defective homologous recombination in BRCA1, BRCA2 and BLM helicase mutants [21–23], because DNA replication stress-associated lesions are primarily the target of homologous recombination.

Here we observed that the escape of G2/M checkpoint with DNA lesions triggers tetraploidy development. Contrary, previous

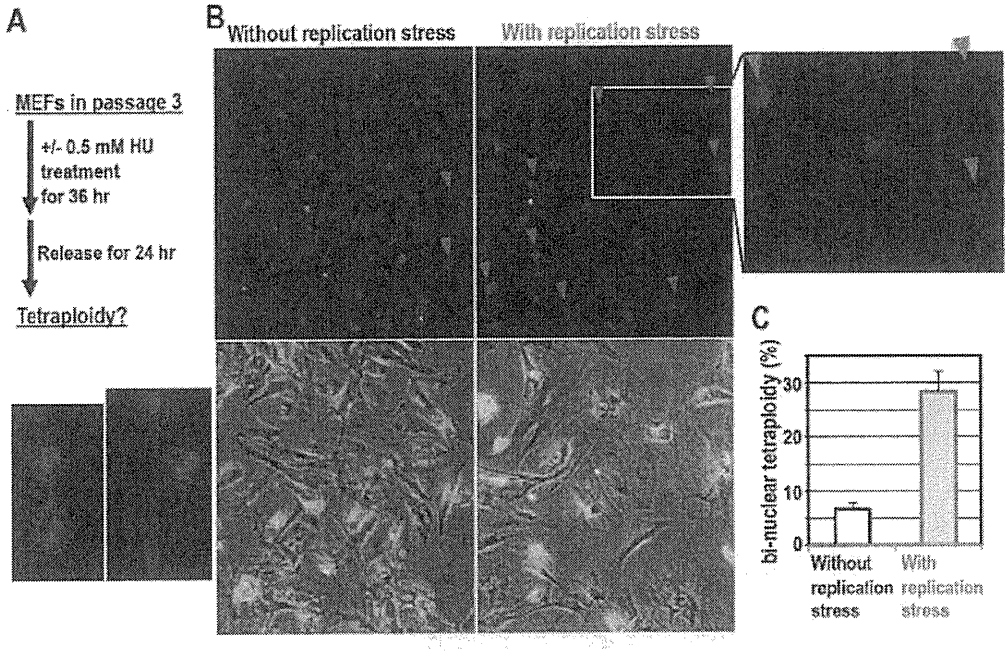

Figure 8. DNA replication stress induces chromosomal bridge formation and tetraploidy in early passage-primary MEFs. A. The effect of DNA replication stress was determined as in the scheme. After transient DNA replication stress, chromosome bridges were often observed. Representative images are shown. **B.** The images are representative with or without DNA replication stress. Arrowheads indicate cells with bi-nuclear tetraploid (red arrowheads). **C.** The proportions of total bi-nuclear cells were estimated. At least 100 cells were counted in each of 3 independent experiments.
doi:10.1371/journal.pone.0008821.g008

reports showed that the identical escape of G2/M checkpoint results in the mitotic catastrophe cell death [24–27]. How the identical DNA lesions could induce completely different effects? Although the mechanistic discrimination is unclear, so far the differences underlie if the cells are in immortal or pre-immortal. In cancer cells, cells with aneuploidy were accumulated after G2/M checkpoint-escape and after the appearance of chromosome bridge (Fig. 1,2). But such aneuploidy accumulates transiently and never come up to major, which was also shown in a previous HeLa cell study [11]. Such transient accumulation of aneuploidy coincided with the increase in sub-G1 fraction (Fig. 2B), suggesting the eventual death induction. In contrast, pre-immortal senescing cells are accumulated with bi-nuclear tetraploidy in association with the escape of G2/M checkpoint, and eventually acquire the immortality, which are totally tetraploidy. In fact, mitotic catastrophe-associated death induction has been mainly studied with the immortalized cells mostly in cancer cell lines, which are described as a goal of cancer therapies. Contrary, somehow pre-immortal cells are resistant to the identical DNA lesions and survive, contributing the development of the immortality.

Prior to acquiring immortality, senescing MEFs are accumulated with a bi-nuclear phenotype that is a primary and transient form of tetraploidy, indicating that such tetraploidy generation in senescing cells is the major event in these stages in association with M-phase DNA lesions, aberrancy in chromosomal segregation and cytokinesis failure. Since immortalized MEFs are totally tetraploidy, these steps must be critical for immortalization. It has been shown that immortalized MEFs are mutated in the Arf/p53 module [17]. We also observed that the Arf/p53 module responds normally in senescing MEFs unlike that in immortalized MEFs (Supplementary Fig. S8), suggesting that the selective pressure of mutants is also coupled with acquiring immortality and tetraploidy development. Here we showed the mechanistic steps of MEFs immortalization, which share with the process of cancer development in many aspects. However, unlike MEFs, primary human cells usually do not show such spontaneous transformation. Difference in MEFs and human cells is mainly because MEFs express TERT and suffer from accelerated growth stimulation with 10% fetal bovine serum, whereas primary human cells require hTERT and the additional acceleration of oncogenes such as Myc, Ras etc. for the immortalization [28,29]. Importantly, our results suggest that the trigger for immortality acquirement-associated development of genomic instability is the precancerous DNA replication stress with oncogene acceleration or with senescence-associated repair deficiency with continuous growth stimulation.

Materials and Methods

Cell Culture, Oncogene Induction, Cell Synchronization, Cell Damage and Replication Stress Induction

Cancer cell lines and normal human fibroblast SuSa were cultured as previously described [30]. MEF cells were prepared as previously described [19]. MEFs were cultured under 3T3 passage protocol [19], in which 3×10^5 MEFs were passed in 6-cm dishes every 3 days using 10% fetal bovine serum containing DMEM (during P1-P6 and after IP1), otherwise maintained with medium-change under the same medium conditions every 3 days (during M1-M7). ER-E2F1 expressing U2OS cells were treated with 4-hydroxytamoxifen (300 nM) as previously described [31]. For transient expression of *Cdc25A*, *Cdc25A* cDNA was inserted into pIREShyg2 vector (Clontech Laboratories, Palo Alto, CA). The

Cdc25A expression vector, empty vector, or none was then transfected into HEK293 cells with FuGENE6. Prometaphase cells were prepared as previously reported [32]. For the preparation of metaphase cells, prometaphase cells were further incubated with 10 μM MG132 for 2 h [33]. These synchronization and chromosome contents were determined with flow cytometry as previously described [32]. DNA double-strand breaks were directly induced by 100 ng/ml NCS (Pola Pharma, Tokyo, Japan) for 10 min or by 2.5 μM adriamycin for 1 h. Induced DNA lesions were detected by γH2AX, which were confirmed with comet assay after NCS treatment (Supplementary Fig. S9). For DNA replication stress-associated DNA-LCM study, SuSa cells were transiently treated with 1 mM HU for 24 h and then released in 10 % FBS DMEM with 20 ng/ml nocodazole for 10 h.

Antibodies, Immunostaining and Western Blotting

Antibodies against γH2AX (JBW301, Upstate Biotechnology) and phospho-histone H3 (Ser 10) (Upstate Biotechnology) were used for immnostaining and Western blot analysis. Antibodies against phospho-ATM (Ser 1981) (10H11.E12, Cell Signaling Technology), phospho-Chk2 (Thr 68) (Cell Signaling Technology), β-actin (AC-74, Sigma), histone H3 (ab1791, Abcam), cyclin B1 (GNS1, Santa Cruz Biotechnology Inc.), p53 (Pab240, Santa Cruz Biotechnology Inc.) and cyclin E (Ab-1, Calbiochem) were used for Western blot analysis. Antibodies against AIM-1 (Aurora-B) (BD Transduction Laboratories), phospho-vimentin (Ser 72) [34], BubR1 (8G1, Upstate Biotechnology) and phospho-ATM (Ser 1981) (clone 7C10D8, Rockland) were used for immunostaining. Before immunostaining with primary and secondary antibodies, cells were fixed with 4% paraformaldehyde for 10 min and permeabilized with 0.1% Triton X-100/PBS for 10 min. For confocal microscope imaging, cells were cultured on coverslips and stained as above. Other immunofluorescence images were captured with ECLIPSE TE300 inverted microscope (Nikon) or LSM510 confocal microscope (Carl Zeiss). Three-dimensional images were constructed with 1 μm-slice pictures of the cells using LSM Image Browser software. Western blot analysis was performed as previously described [32].

Immunofluorescence and Time-Lapse Imaging

Fifteen hours after the release from M phase-DNA damage, cells were fixed with 10% neutral buffered formalin for 10 min, permeabilized with 0.3% Triton X-100/PBS for 10 min, and stained with DAPI for 5 min. Phase contrast images merged with immunofluorescence images were captured with ECLIPSE TE300 inverted microscope. Time-lapse images were acquired with Multicell-imaging incubator (Sanyo).

Comet Assay

A comet assay was performed as previously described [32].

Chromosome Spreads

Mitotic cells were prepared in a 6-h treatment with 20 ng/ml nocodazole and shaking-off. The collected cells were hypotonically swollen with 75 mM KCl for 15 min, and then fixed with −20°C Carnoy's solution (75% methanol/25% acetic acid) for 20 min. The fixative was changed once and the cells in Carnoy's solution were dropped onto glass slides and air-dried. The slides were stained with 4% Giemsa (Merck) solution for 10 min, washed briefly in tap water, and air-dried.

Supporting Information

Movie S1 Movies S1-S4. For the precise investigation of the process of tetraploidy development in the M-phase cells with DNA lesions, time-lapse imaging was performed. After cells were damaged with NCS as in Fig. 5A, the damaged cells (Movies S2 and S4) or non-damaged control (Movies S1 and S3) were monitored with close-up views (Movies S1 and S2) or wide-range views (Movies S3 and S4). The images shown in Fig. 5B are from those in Movies S1 and S2.
Found at: doi:10.1371/journal.pone.0008821.s001 (0.27 MB MOV)

Movie S2 Movies S1-S4. For the precise investigation of the process of tetraploidy development in the M-phase cells with DNA lesions, time-lapse imaging was performed. After cells were damaged with NCS as in Fig. 5A, the damaged cells (Movies S2 and S4) or non-damaged control (Movies S1 and S3) were monitored with close-up views (Movies S1 and S2) or wide-range views (Movies S3 and S4). The images shown in Fig. 5B are from those in Movies S1 and S2.
Found at: doi:10.1371/journal.pone.0008821.s002 (0.27 MB MOV)

Movie S3 Movies S1-S4. For the precise investigation of the process of tetraploidy development in the M-phase cells with DNA lesions, time-lapse imaging was performed. After cells were damaged with NCS as in Fig. 5A, the damaged cells (Movies S2 and S4) or non-damaged control (Movies S1 and S3) were monitored with close-up views (Movies S1 and S2) or wide-range views (Movies S3 and S4). The images shown in Fig. 5B are from those in Movies S1 and S2.
Found at: doi:10.1371/journal.pone.0008821.s003 (1.41 MB MOV)

Movie S4 Movies S1-S4. For the precise investigation of the process of tetraploidy development in the M-phase cells with DNA lesions, time-lapse imaging was performed. After cells were damaged with NCS as in Fig. 5A, the damaged cells (Movies S2 and S4) or non-damaged control (Movies S1 and S3) were monitored with close-up views (Movies S1 and S2) or wide-range views (Movies S3 and S4). The images shown in Fig. 5B are from those in Movies S1 and S2.
Found at: doi:10.1371/journal.pone.0008821.s004 (1.09 MB MOV)

Figure S1 Hypothesis. Cells damaged with precancerous DNA lesions develop tetraploidy hypothetically via chromosomal bridges during chromosomal segregation (bottom), unlike cell division in cells without DNA lesions (top). If this is the case, generated cells with tetraploidy are primarily and transiently bi-nuclear until the following M phase, in which daughter chromosomes assemble in a common metaphase plate to lead into tetraploidy with a single nucleus in the subsequent G1 phase.
Found at: doi:10.1371/journal.pone.0008821.s005 (3.03 MB TIF)

Figure S2 Transient over-expression of Cdc25A promotes DNA lesions including the cells during mitosis. Empty (control) or Cdc25A expression (Cdc25A) vectors were transfected into HEK293 cells. After cultivation for two days, cells were determined with the indicated antibodies.
Found at: doi:10.1371/journal.pone.0008821.s006 (3.02 MB TIF)

Figure S3 Tetraploidy generation with DNA damage during mitosis in U2OS, WI-38 and primary MEFs. A. Cells prepared as in the experimental scheme on Fig. 5A were stained with DAPI. The arrowheads indicate bi-nuclear tetraploid cells. B. Quantification of the tetraploid cells was performed with at least 100 cells for each.
Found at: doi:10.1371/journal.pone.0008821.s007 (2.99 MB TIF)

Figure S4 Cells damaged during mitosis lead to tetraploidy generation but not during interphase. HeLa cells in the M phase or without synchronization were treated as in the scheme. Unlike

asynchronous cells, M phase-cells specifically develop tetraploidy after damage. Quantification of the tetraploid cells was performed with at least 100 cells for each.
Found at: doi:10.1371/journal.pone.0008821.s008 (2.21 MB TIF)

Figure S5 The cells damaged in the M phase further replicate DNAs in the following S phase. A,B. After cells were damaged with NCS (A) or adriamycin (B) as in Fig. 5A, the chromosome contents of the cells after the release were analyzed by flow cytometry.
Found at: doi:10.1371/journal.pone.0008821.s009 (1.10 MB TIF)

Figure S6 DNA damage checkpoint activation is durable in the M phase, but dysfunctional to induce arrest during mitosis. The activation of DNA damage checkpoint protein Chk2 in the HeLa asynchronous and M-phase cells characterized by phosphorylated histone H3 (P-H3) was analyzed for the phosphorylated form.
Found at: doi:10.1371/journal.pone.0008821.s010 (0.37 MB TIF)

Figure S7 Prometaphase-DNA damage does not affect the behavior of BubR1 and the progression into the anaphase and the telophase. At 75 min after the release from NCS treatment as in the experimental scheme on Fig. 5A, the cells were stained with anti-BubR1 antibody and DAPI. For the NCS-treated cells, the mitotic stages in the anaphase and the telophase are estimated based on the degree of cell elongation.

Found at: doi:10.1371/journal.pone.0008821.s011 (4.78 MB TIF)

Figure S8 Arf/p53 module mutation in the immortalized MEFs. To determine the loss of Arf/p53 module, p53 accumulation was monitored 12 h after 100 ng/ml NCS treatment at each stage of MEFs: primary growth (P4); senescence (M2); immortalized (IP2).
Found at: doi:10.1371/journal.pone.0008821.s012 (0.63 MB TIF)

Figure S9 DNA lesions indicated by γH2AX were also confirmed with comet assay. DNA lesions, indicated by γH2AX in this study, were also confirmed by comet assay with the tails after NCS treatment for 15 min. Arrow heads indicate the spots with comet tails, indicating DNA damages.
Found at: doi:10.1371/journal.pone.0008821.s013 (2.88 MB TIF)

Acknowledgments

We thank K Helin for kindly providing ER-E2F1-expressing U2OS cells.

Author Contributions

Conceived and designed the experiments: YI KiY. Performed the experiments: YI KiY YY KS HF JU. Analyzed the data: KiY MT HG MI SM HT. Contributed reagents/materials/analysis tools: MT HG MI. Wrote the paper: KiY HT.

References

1. Lengauer C, Kinzler KW, Volgelstein B (1997) Genetic instability in colorectal cancers. Nature 386: 623–627.
2. Bartkova J, Horejsí Z, Koed K, Krämer A, Tort F, et al. (2005) DNA damage response as a candidate anti-cancer barrier in early human tumorigenesis. Nature 434: 864–870.
3. Gorgoulis VG, Vassiliou LV, Karakaidos P, Zacharatos P, Kotsinas A, et al. (2005) Activation of the DNA damage checkpoint and genomic instability in human precancerous lesions. Nature 434: 907–913.
4. Lengauer C, Kinzler KW, Vogelstein B (1998) Genetic instabilities in human cancers. Nature 396: 643–649.
5. Ganem NJ, Storchova Z, Pellman D (2007) Tetraploidy, aneuploidy and cancer. Curr Opin Genet Dev 17: 157–162.
6. Shi Q, King RW (2005) Chromosome nondisjunction yields tetraploid rather than aneuploid cells in human cell lines. Nature 437: 1038–1042.
7. Fujiwara T, Bandi M, Nitta M, Ivanova EV, Bronson RT, et al. (2005) Cytokinesis failure generating tetraploids promotes tumorigenesis in p53-null cells. Nature 437: 1043–1047.
8. Musacchio A, Salmon ED (2007) The spindle-assembly checkpoint in space and time. Nat Rev Mol Cell Biol 8: 379–393.
9. Weaver BA, Silk AD, Montagna C, Verdier-Pinard P, Cleveland DW (2007) Aneuploidy acts both oncogenically and as a tumor suppressor. Cancer Cell 11: 25–36.
10. Sotillo R, Hernando E, Díaz-Rodríguez E, Teruya-Feldstein J, Cordón-Cardo C, et al. (2007) Mad2 overexpression promotes aneuploidy and tumorigenesis in mice. Cancer Cell 11: 9–23.
11. Steigemann P, Wurzenberger C, Schmitz MHA, Held M, Guizetti J, et al. (2009) Aurora B-mediated abscission checkpoint protects against tetraploidization. Cell 136: 473–484.
12. Deckbar D, Birraux J, Krempler A, Tchouandong L, Beucher A, et al. (2007) Chromosome breakage after G2 checkpoint release. J Cell Biol 176: 749–755.
13. Huang X, Tran T, Zhang L, Hatcher R, Zhang P (2005) DNA damage-induced mitotic catastrophe is mediated by the Chk1-dependent mitotic exit DNA damage checkpoint. Proc Nat Acad Sci USA 102: 1065–1070.
14. Mikhailov A, Cole RW, Rieder CL (2002) DNA damage during mitosis in human cells delays the metaphase/anaphase transition via the spindle-assembly checkpoint. Curr Biol 12: 1797–1806.
15. Carmena M, Earnshaw WC (2003) The cellular geography of aurora kinases. Nat Rev Mol Cell Biol 4: 842–854.
16. McCollum D (2004) Cytokinesis: the central spindle takes center stage. Curr Biol 14: R953–R955.
17. Matheu A, Maraver A, Klatt P, Flores I, Garcia-Cao I, et al. (2007) Delayed ageing through damage protection by the Arf/p53 pathway. Nature 448: 375–379.
18. Sedelnikova OA, Horikawa I, Zimonjic DB, Popescu NC, Bonner WM, et al. (2004) Senescing human cells and ageing mice accumulate DNA lesions with unrepairable double-strand breaks. Nature Cell Biol 6: 168–170.
19. Todaro GJ, Green H (1963) Quantitative studies of the growth of mouse embryo cells in culture and their development into established lines. J Cell Biol 17: 299–313.
20. Nakada S, Katsuki Y, Imoto I, Yokoyama T, Nagasawa M, et al. (2006) Early G2/M checkpoint failure as a molecular mechanism underlying etoposide-induced chromosomal aberrations. J Clin Invest 116: 80–89.
21. Scully R, Livingston DM (2000) In search of the tumour-suppressor functions of BRCA1 and BRCA2. Nature 408: 429–432.
22. Powell SN, Kachnic LA (2003) Roles of BRCA1 and BRCA2 in homologous recombination, DNA replication fidelity and the cellular response to ionizing radiation. Oncogene 22: 5784–5791.
23. Tripathi V, Nagarjuna T, Sengupta S (2007) BLM helicase-dependent and -independent roles of 53BP1 during replication stress-mediated homologous recombination. J Cell Biol 178: 9–14.
24. Chan TA, Hermeking H, Lengauer C, Kinzler KW, Vogelstein B (1999) 14-3-3σ is required to prevent mitotic catastrophe after DNA damage. Nature 401: 616–620.
25. Roninson IB, Broude EV, Chang BD (2001) If not apoptosis, then what? Treatment-induced senescence and mitotic catastrophe in tumor cells. Drug Resist Update 4: 303–313.
26. Nitta M, Kobayashi O, Honda S, Hirota T, Kuninaka S, et al. (2004) Spindle checkpoint function is required for mitotic catastrophe induced by DNA-damaging agents. Oncogene 23: 6548–6558.
27. Reinhardt HC, Aslanian AS, Lees JA, Yaffe MB (2007) p53-deficient cells rely on ATM- and ATR-mediated checkpoint signaling through the p38MAPK/MK2 pathway for survival after DNA damage. Cancer Cell 11: 175–189.
28. Narisawa-Saito M, Handa K, Yugawa T, Ohno S, Fujita M, et al. (2007) HPV16 E6-mediated stabilization of ErbB2 in neoplastic transformation of human cervical keratinocytes. Oncogene 26: 2988–2996.
29. Sasaki R, Narisawa-Saito M, Yugawa T, Fujita M, Tashiro H, et al. (2009) Oncogenic transformation of human ovarian surface epithelial cells with defined cellular oncogenes. Carcinogenesis 30: 423–431.
30. Yoshioka K, Yoshioka Y, Hsieh P (2006) ATR kinase activation mediated by MutSα and MutLα in response to cytotoxic O^6-methylguanine adducts. Mol Cell 22: 501–510.
31. Müller H, Bracken AP, Vernell R, Moroni MC, Christians F, et al. (2001) E2Fs regulate the expression of genes involved in differentiation, development, proliferation, and apoptosis. Genes Dev 15: 267–285.
32. Ichijima Y, Sakasai R, Okita N, Asahina K, Mizutani S, et al. (2005) Phosphorylation of histone H2AX at M phase in human cells without DNA damage response. Biochem Biophys Res Commun 336: 807–812.
33. Petronczki M, Glotzer M, Kraut N, Peters JM (2007) Polo-like kinase 1 triggers the initiation of cytokinesis in human cells by promoting recruitment of the RhoGEF Ect2 to the central spindle. Dev Cell 12: 713–725.
34. Goto H, Yasui Y, Kawajiri A, Nigg EA, Terada Y, et al. (2003) Aurora-B regulates the cleavage furrow-specific vimentin phosphorylation in the cytokinetic process. J Biol Chem 278: 8526–8530.

Genes to Cells

DPPA4 modulates chromatin structure via association with DNA and core histone H3 in mouse embryonic stem cells

Hisaharu Masaki[1,2], Tomohiro Nishida[1a], Ryo Sakasai[1]* and Hirobumi Teraoka[1]

[1]*Department of Pathological Biochemistry, Medical Research Institute, Tokyo Medical and Dental University, Chiyoda-ku, Tokyo 101-0062, Japan*

[2]*Research Fellow of the Japan Society for the Promotion of Science, Japan*

Developmental pluripotency associated 4 (DPPA4) is one of the uncharacterized genes that is highly expressed in embryonic stem (ES) cells. DPPA4 is associated with active chromatin and involved in the pluripotency of mouse ES cells. However, the biological function of DPPA4 remains poorly understood. In this study, we performed fluorescence recovery after photobleaching (FRAP) analysis to examine the dynamics of DPPA4 in ES cells. FRAP analysis showed that the mobility of DPPA4 is similar to that of histone H1. In addition, biochemical analysis with purified proteins and immunoprecipitation analysis showed that DPPA4 directly binds to both DNA and core histone H3. The analysis using truncated proteins indicated that DPPA4 is associated with DNA via the N-terminal region and histone H3 via the C-terminal region. *In vitro* assembled chromatin showed resistance to micrococcal nuclease (MNase) digestion in the presence of DPPA4. Moreover, MNase assay and FRAP analysis with the truncated proteins implies that DPPA4 binding to both DNA and histone H3 is necessary for the chromatin structure resistant to MNase and for the proper localization of DPPA4 in ES cell nuclei. These results suggest that DPPA4 modulates the chromatin structure in association with DNA and histone H3 in ES cells.

Introduction

Mouse embryonic stem (ES) cells, derived from the inner cell mass of the blastocyst, have unlimited capacity for self-renewal and can differentiate into various cell types (Keller 2005). Moreover, human ES cells and induced pluripotent stem (iPS) cells have been established (Thomson *et al.* 1998; Takahashi *et al.* 2007; Yu *et al.* 2007). Thus, they are expected to become a valuable resource for stem cell therapy.

The pluripotency of mouse ES cells is maintained by the leukemia inhibitory factor (LIF) Jak/STAT3, bone morphogenic protein (BMP) Smad/Id, and Wnt/β-catenin signaling pathways (Burdon *et al.* 2002; Boiani & Schöler 2005). In addition, several transcription factors including Oct-3/4, Sox-2, Nanog, Sall4, and Klf family proteins play essential roles in mouse ES cell pluripotency (Chambers *et al.* 2003; Mitsui *et al.* 2003; Niwa *et al.* 2005; Zhang *et al.* 2006; Masui *et al.* 2007; Jiang *et al.* 2008). These signaling pathways and core transcription factors synergistically contribute to the maintenance of pluripotency in mouse ES cells, e.g., the LIF/Jak/STAT3 signaling pathway maintains ES cells in an undifferentiated state by the regulation of Klf4 gene expression (Niwa *et al.* 2009).

Genes involved in ES cell pluripotency and many other genes including Dppa4 (developmental pluripotency associated 4) are highly expressed during early mouse embryogenesis (Hamatani *et al.* 2004). Dppa4 is one of the genes originally identified as being highly expressed in early mouse embryo and ES cells (Bortvin *et al.* 2003). It has been reported that the expression of Dppa4 gene is potentially regulated by Oct-3/4 and Sox-2 in ES cells (Boyer *et al.* 2005; Chakravarthy *et al.* 2008). The expression of Dppa4 gene is restricted to early embryo and germ cells (Maldonado-Saldivia *et al.* 2007). DPPA4 has the SAP (SAF-A/B, Acinus and PIAS) domain, which is a putative

Communicated by: Kohei Miyazono

**Correspondence:* sakasai.pbc@mri.tmd.ac.jp

[a]*Present address*: Department of Stem Cell Medicine, Medical Research Institute, Tokyo Medical and Dental University, Chiyoda-ku, Tokyo 101-0062, Japan.

DOI: 10.1111/j.1365-2443.2010.01382.x

DNA-binding motif, and is considered to be involved in chromosomal organization, RNA processing, DNA repair, and apoptotic degradation of chromatin (Aravind & Koonin 2000). Several genes including Dppa4 have been identified by the RNAi screening against the requirement for self-renewal in mouse ES cells (Ivanova *et al.* 2006). Thus, it is considered that DPPA4 plays an important role in ES cells via association with chromatin. In fact, we have previously reported that DPPA4 associated with active chromatin is required for maintaining mouse ES cells in an undifferentiated state (Masaki *et al.* 2007).

Recent studies have revealed that unique chromatin states are maintained in ES cells. Major architectural chromatin proteins, such as histone H1, loosely bind to chromatin (Meshorer *et al.* 2006). The promoters of some developmental regulator genes have bivalent chromatin profiles in which both active (tri-methylation of histone H3 at lysine 4) and inactive (tri-methylation of histone H3 at lysine 27) chromatin marks are juxtaposed (Azuara *et al.* 2006; Bernstein *et al.* 2006). In addition, Polycomb repressive complex 2 (PRC2) binds to promoters of the developmental regulator genes and represses their transcription in ES cells (Boyer *et al.* 2006; Lee *et al.* 2006). The proteasome promotes a dynamic turnover of transcription factors and RNA polymerase II binding at tissue-specific genes, thereby restricting permissive transcriptional activity and keeping the genes in a potentiated state (Szutorisz *et al.* 2006). These reports indicate that ES cells have a unique open chromatin structure and suggest that pluripotency and differentiation are regulated by chromatin states. Thus, DPPA4 is associated with chromatin and possibly involved in the unique chromatin structure of ES cells.

In this study, to gain an insight into the molecular function of DPPA4 in mouse ES cells, we investigated the behavior of DPPA4 by fluorescence recovery after photobleaching (FRAP) analysis. Interestingly, FRAP analysis showed that the mobility of DPPA4 was similar to that of histone H1. Purified recombinant DPPA4 protein directly binds to DNA and core histones *in vitro*, and immunoprecipitation analysis showed the binding between DPPA4 and histone H3 in ES cells. The analysis of truncated DPPA4 proteins revealed that DPPA4 binds to DNA and histone H3 via the N-terminal and C-terminal regions, respectively. Furthermore, the addition of DPPA4 into *in vitro* reconstituted chromatin resulted in an increased resistance to micrococcal nuclease (MNase) digestion. Based on these results, we proposed a model that DPPA4 modulates the chromatin structure in association with DNA and histone H3 in ES cells.

Results

DPPA4 shows similar dynamics to linker histone H1

DPPA4 is involved in the maintenance of pluripotency in ES cells, but its function remains to be clarified. The putative SAP DNA-binding domain of DPPA4 raises a possibility that DPPA4 contributes to DNA metabolism through binding to chromatin. To investigate the molecular function of DPPA4 on chromosomal organization, we analyzed the dynamic property of DPPA4 and compared it with that of histones in living ES cells using FRAP analysis. As a preliminary experiment for FRAP analysis, the localization of DPPA4-EGFP (enhanced green fluorescent protein [GFP]) fusion protein was compared with that of endogenous DPPA4 by chromatin fractionation and cytochemistry detecting EGFP. Western blot analysis showed 42-kDa (DPPA4) and 75-kDa (DPPA4-EGFP) bands in ES cells transfected with DPPA4-EGFP expression vector, and the latter was not detected in mock-transfected cells (Fig. 1A). We carried out chromatin fractionation by increasing salt concentration. In the presence of 150 mM NaCl, DPPA4-EGFP, DPPA4, and core histone H3 were hardly solubilized, while a linker histone H1 was slightly solubilized (Fig. 1B). By addition of 500 mM NaCl, DPPA4-EGFP, DPPA4, and histone H1 were mostly solubilized, whereas histone H3 was retained in chromatin even under high-salt conditions (Fig. 1B). This suggests that DPPA4 is a chromatin factor showing a similar behavior to linker histone H1, but not core histone H3. DPPA4-EGFP, as well as endogenous DPPA4, localizing in chromatin during both the interphase and mitotic phase (Fig. 1D and F), suggesting that the localization of DPPA4-EGFP in ES cells corresponds to that of endogenous DPPA4. Taken together, these data suggest that DPPA4 is a chromatin factor like histone H1 rather than core histones.

Using ES cells transiently transfected with DPPA4-EGFP, linker histone $H1^0$-EGFP, and core histone H3-EGFP expression vectors, FRAP analysis was performed. In ES cells expressing histone H3-EGFP, fluorescence of bleaching strip was hardly recovered 120 s after bleaching, indicating that histone H3 is actually an immobile protein (Fig. 2A). In contrast, in ES cells expressing histone $H1^0$-EGFP or DPPA4-EGFP, fluorescence of bleaching strip gradually

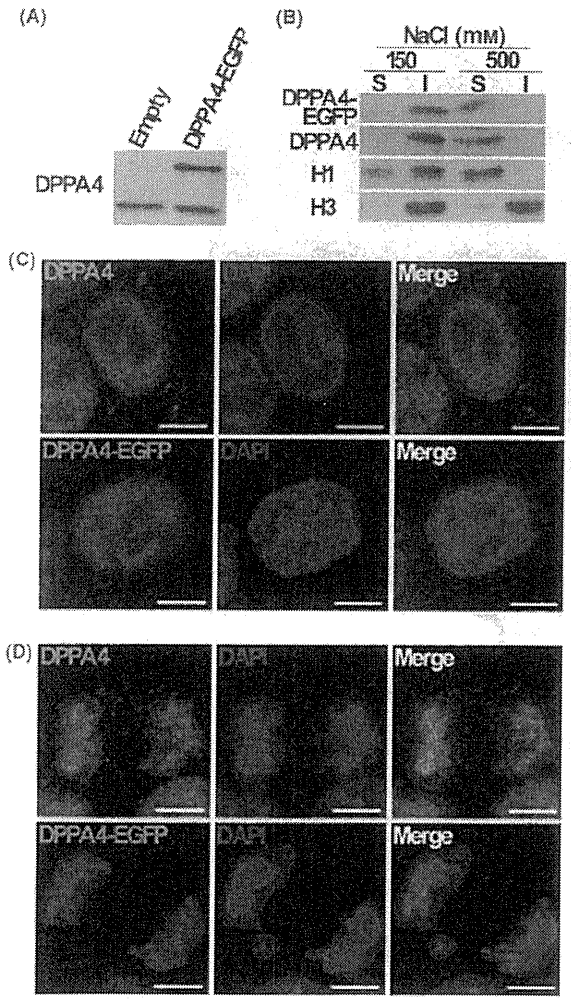

Figure 1 Cellular localization of developmental pluripotency associated 4 (DPPA4)-EGFP in embryonic stem (ES) cells. (A) Western blot analysis of DPPA4-EGFP expression in chromatin fraction of ES cells transfected with DPPA4-EGFP or empty vector. (B) Western blot analysis for DPPA4-EGFP, endogenous DPPA4, histone H1 and H3 in soluble (S) and insoluble (I) fractions of ES cells treated with the buffer containing 150 mM and 500 mM NaCl. (C–D) Confocal images of interphase (C) or metaphase (D) ES cells, showing endogenous DPPA4 immunostained with anti-DPPA4 antibodies (green; upper) and fluorescent DPPA4-EGFP (green; lower). Nuclei were counterstained with 4′,6′-diamino-2-phenylindole (DAPI, blue). Scale bars, 5 μm.

recovered within 120 s, indicating that DPPA4 and histone $H1^0$ are mobile proteins compared with histone H3. The time-dependent changes in fluorescence intensity of the bleaching strip in these cells were plotted versus the pre-bleach level to produce FRAP recovery curves. The histone H3 signal scarcely recovered (Fig. 2B), whereas DPPA4 and histone H1 showed gradual recovery after bleaching (Fig. 2C,D). Interestingly, FRAP recovery curves merged with DPPA4-EGFP, and histone $H1^0$-EGFP showed that the mobility of DPPA4 is very similar to that of histone $H1^0$ mobility in living ES cells (Fig. 2E).

DPPA4 directly binds to DNA *in vitro*

Next, to investigate the biochemical function of DPPA4, we purified recombinant DPPA4-His_6 protein expressed in *E. coli* (Fig. 3A). With the use of purified DPPA4, gel shift assay was performed to examine whether DPPA4 directly binds to DNA. Purified DPPA4 and pBluescript DNA were mixed and the protein–DNA complex was analyzed by agarose gel electrophoresis. As shown in Fig. 3B, the bands were stepwise shifted in a DPPA4 amount-dependent manner. These results are consistent with the previous report that DPPA4 has the SAP DNA-binding domain (Aravind & Koonin 2000). Stella/DPPA3, which has the SAP domain, binds to methylated DNA *in vitro* and protects against DNA demethylation in early mouse embryo (Nakamura *et al.* 2007). To investigate the effect of DNA methylation on the DNA-binding capacity of DPPA4, CpG sites of plasmid DNA were methylated by the CpG methylase *Sss* I. Methylated plasmid DNA showed resistance to digestion of *Hap II*, a methylation sensitive restriction enzyme (data not shown). Gel shift assay showed that DPPA4 binds to methylated plasmid DNA as well as non-methylated plasmid DNA (Fig. 3C), suggesting that DNA methylation does not affect DNA binding of DPPA4.

DPPA4 directly binds to histone H3 *in vitro* and *in vivo*

DPPA4 is considered a chromatin factor, providing the possibility of the association between DPPA4 and core histones. To examine whether DPPA4 directly binds to core histone proteins (H2A, H2B, H3 and H4) *in vitro*, we carried out Far-Western blotting analysis. Core histone proteins were purified from ES cells (Fig. 4A), and were used as a prey protein in Far-Western blotting analysis with purified DPPA4. As shown in Fig. 4B, histone H3 and H2B were detected, but neither H2A nor H4 bands. In case of using DPPA4 as a prey protein, the DPPA4 band was

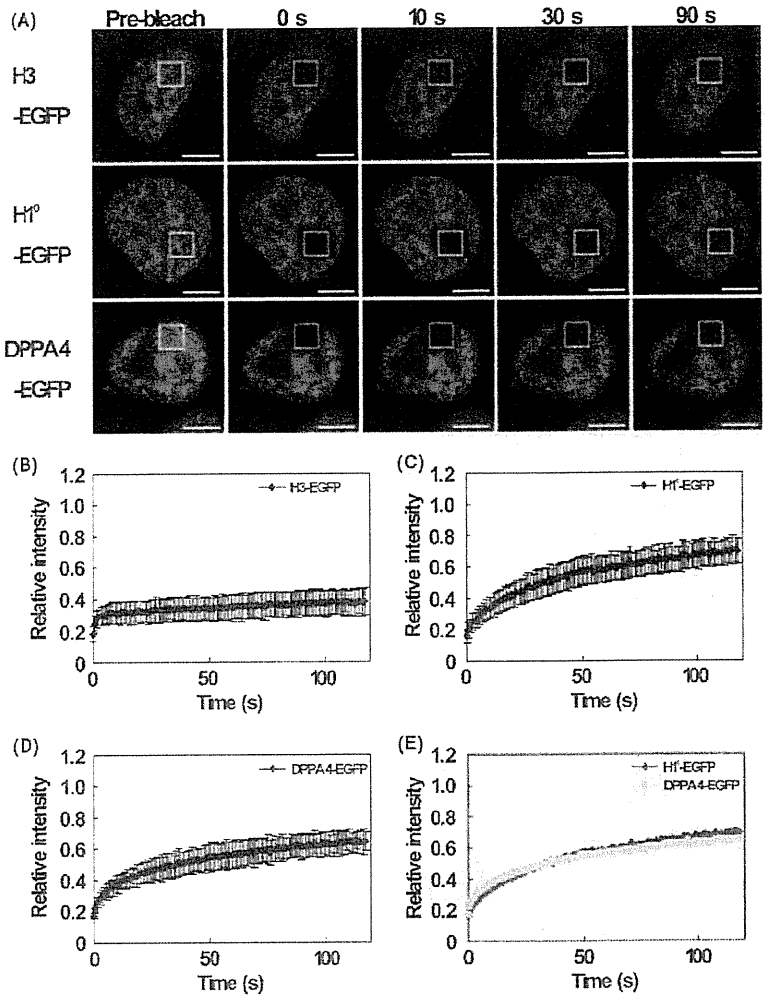

Figure 2 Fluorescence recovery after photobleaching (FRAP) analysis of developmental pluripotency associated 4 (DPPA4)-EGFP, histone $H1^0$-EGFP, and H3-EGFP in embryonic stem (ES) cells. (A) Representative images of FRAP analysis in living ES cells transfected with histone H3-EGFP, $H1^0$-EGFP, or DPPA4-EGFP expression vector. The bleach areas are marked with white squares. The fluorescence recovery was monitored and shown at indicated time points after bleaching. Scale bars, 5 μm. (B–D) Quantitative FRAP analysis (FRAP recovery curves) of transiently expressed histone H3-EGFP (B), $H1^0$-EGFP (C), and DPPA4-EGFP (D) in ES cells. Each value is the mean ± SD. (E) Comparison of FRAP recovery curves between ES cells expressing histone $H1^0$-EGFP (blue) and DPPA4-EGFP (yellow).

detected in a reciprocal experiment with histone H3 (data not shown). These data suggest that DPPA4 binds to histone H3 and H2B *in vitro*. To confirm DPPA4 binding to core histones, we performed *in vitro* co-immunoprecipitation using purified recombinant DPPA4 and core histone proteins with anti-DPPA4 antibodies. In the presence of histone H3 and H4, histone H3 was co-immunoprecipitated with anti-DPPA4 antibodies, but not with non-immune IgG (Fig. 4C). These results suggest direct binding between DPPA4 and histone H3 *in vitro*.

To investigate whether DPPA4 directly binds to core histone proteins in ES cells, co-immunoprecipitation between DPPA4 and core histones was performed using ES cell extracts. Whole ES cell extracts were sonicated to disrupt the nucleosome structure, and used for immunoprecipitation assay. DPPA4 was immunoprecipitated with histone H3 in ES cells,

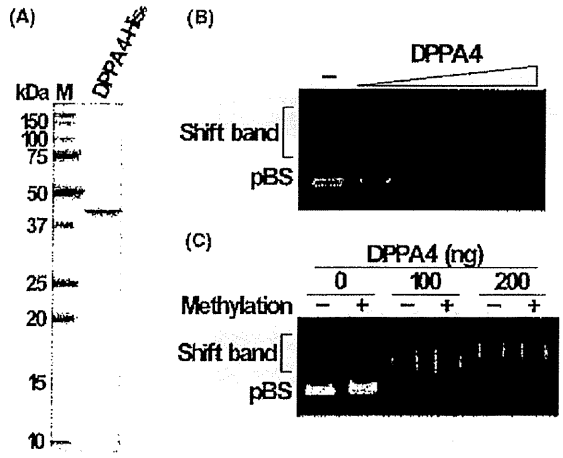

Figure 3 Gel shift analysis using developmental pluripotency associated 4 (DPPA4)-His_6. (A) Coomassie brilliant blue staining of the purified recombinant DPPA4-His_6 protein from *E. coli*. M, molecular mass markers. (B) Gel shift assay with plasmid DNA (pBlueScript II SK+; pBS) and increasing amount of DPPA4-His_6, (0, 100, 200, 400, and 800 ng). (C) Gel shift assay with methylated or non-methylated plasmid DNA (pBS) and increasing amount of recombinant DPPA4-His_6 (0, 100, and 200 ng).

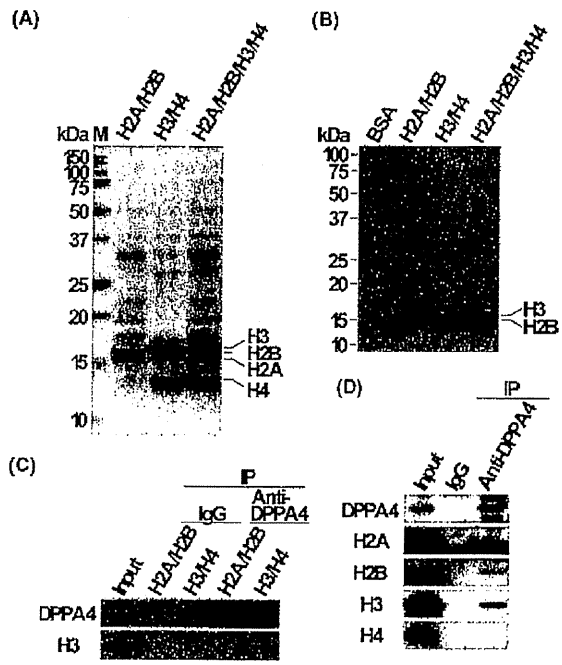

Figure 4 Interaction between developmental pluripotency associated 4 (DPPA4) and core histones *in vitro* and *in vivo*. (A) Coomassie brilliant blue staining of purified H2A/H2B, H3/H4, and H2A/H2B/H3/H4 from embryonic stem (ES) cells. M, molecular mass markers. (B) Far western blotting analysis using recombinant DPPA4-His_6 and purified histones as a bait- and prey protein, respectively. The bands were detected with anti-DPPA4 antibodies. Numbers on the left side of the gel indicate the position of marker proteins. (C) Western blot analysis of *in vitro* co-immunoprecipitation (IP) using purified core histones (H2A + H2B, H3 + H4) and recombinant DPPA4-His_6 by anti-DPPA4 antibodies or control IgG. The bands in input and IPs were detected with anti-DPPA4 or anti-H3 antibodies. (D) Western blot analysis of co-immunoprecipitation (IP) by anti-DPPA4 antibodies or control IgG with ES cell extracts. The bands in input and IPs were detected with anti-DPPA4, anti-H2A, anti-H2B, anti-H3, and anti-H4 antibodies.

whereas H2B was only slightly detected, and the others were not (Fig. 4D). These data suggest that DPPA4 is mainly associated with histone H3 in ES cells.

DPPA4 binds to DNA via the N-terminal region and to histone H3 via the C-terminal region

Next, to determine the DPPA4 regions mediating interactions with DNA and histone H3, we purified two truncated proteins, DPPA4 N-terminal region (DPPA4ΔC-His_6) containing the SAP domain and C-terminal region (DPPA4ΔN-His_6) (Fig. 5A,B). Using purified wild-type (wt) DPPA4 and truncated proteins, gel shift assay was performed. In the presence of DPPA4ΔC as well as wt DPPA4, the bands were stepwise shifted in a protein amount-dependent manner, whereas the bands were slightly shifted in the presence of DPPA4ΔN (Fig. 5C). These results suggest that the N-terminal region of DPPA4 has a greater binding affinity for DNA than the C-terminal region.

Likewise, we performed *in vitro* immunoprecipitation using these truncated proteins and total core histones with anti-6xHis antibodies. Histone H3 was efficiently precipitated with DPPA4ΔN compared with DPPA4 wt and DPPA4ΔC (Fig. 5D), indicating that the binding affinity of the C-terminal region of DPPA4 for histone H3 is higher than that of the N-terminal region. Taken together, these results suggest that DPPA4 associates with DNA and histone H3 via the N- and C-terminal regions, respectively.

DPPA4 modulates chromatin structure *in vitro*

Because a similar mobility of DPPA4 to linker histone $H1^0$ and DPPA4 binding to both DNA and

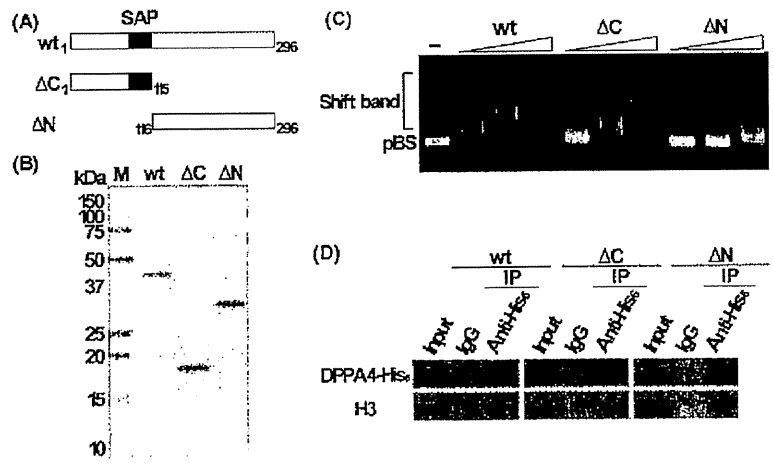

Figure 5 Binding analysis of truncated developmental pluripotency associated 4 (DPPA4) proteins to DNA or histone H3 *in vitro*. (A) Schematic representation of wild-type (wt) and truncated DPPA4 proteins (ΔC, ΔN). The SAP domain (amino acids 81–115) is depicted by the black box. (B) Coomassie brilliant blue staining of the purified recombinant wt DPPA4-His_6, DPPA4ΔC-His_6, and DPPA4ΔN-His_6 proteins from *E. coli*. M, molecular mass markers. (C) Gel shift assay with plasmid DNA (pBS) and increasing amount of DPPA4-His_6, DPPA4ΔC-His_6, or DPPA4ΔN-His_6 (100, 200, and 400 ng). (D) Western blot analysis of *in vitro* co-immunoprecipitation (IP) using purified H2A/H2B/H3/H4 and DPPA4-His_6, DPPA4ΔC-His_6, or DPPA4ΔN-His_6 by anti-His_6 antibodies or control IgG. The bands in input and IPs were detected with anti-6xHis (DPPA4) and anti-H3 antibodies (H3).

histone H3 were revealed, we hypothesized that DPPA4 modulates the chromatin structure like histone H1. Thus, we investigated whether the chromatin structure is affected by DPPA4 using *in vitro* reconstituted chromatin. *In vitro* reconstituted chromatin was incubated with purified histone $H1^0$ and DPPA4 (Fig. 6A), followed by digestion with MNase. The addition of histone $H1^0$ enhanced the resistance to MNase digestion compared to the addition of BSA (Fig. 6B), as previously reported (Kim *et al.* 2004). Similar to histone H1, the addition of DPPA4-His_6 resulted in an increase in the resistance to MNase digestion (Fig. 6B). These results indicate that DPPA4 incorporated into the reconstituted chromatin promoted the formation of nuclease-resistant chromatin structure like histone H1 and imply that DPPA4 modulates the chromatin structure in ES cells.

We further investigated whether the formation of nuclease-resistant chromatin structure requires DPPA4 binding to either DNA, histone H3 or both DNA and H3, using truncated DPPA4 proteins (Fig. 5A,B). The addition of DPPA4ΔC or DPPA4ΔN resulted in a decrease in the resistance to MNase digestion compared with wt DPPA4 (Fig. 6C). These results suggest that the DPPA4 binding to both DNA and histone H3 is required for the formation of nuclease-resistant chromatin structure.

Binding to both DNA and histone H3 is required for the proper dynamics of DPPA4 in ES cells

Finally, to investigate whether binding of DPPA4 to DNA and histone H3 affects the localization and mobility of DPPA4 in ES cells, we performed localization and FRAP analyses using truncated DPPA4-EGFP fusion proteins. The localization of truncated DPPA4-EGFP fusion proteins was compared with that of wt DPPA4 in ES cells. Confocal microscopy showed nuclear localization of DPPA4ΔC-EGFP and DPPA4ΔN-EGFP as well as DPPA4 wt-EGFP (Fig. 7A). DPPA4 wt-EGFP and DPPA4ΔN-EGFP were not localized in nucleoli, whereas DPPA4ΔC-EGFP was diffusely distributed in an entire nucleus (Fig. 7A).

In ES cells transiently transfected with DPPA4 wt-EGFP, DPPA4ΔC-EGFP, and DPPA4ΔN-EGFP expression vectors, FRAP analysis was performed. FRAP analysis showed that DPPA4ΔC-EGFP and DPPA4ΔN-EGFP signals were immediately recovered in contrast to the DPPA4 wt-EGFP signal (Fig. 7B–E). These data indicate that DPPA4 binding

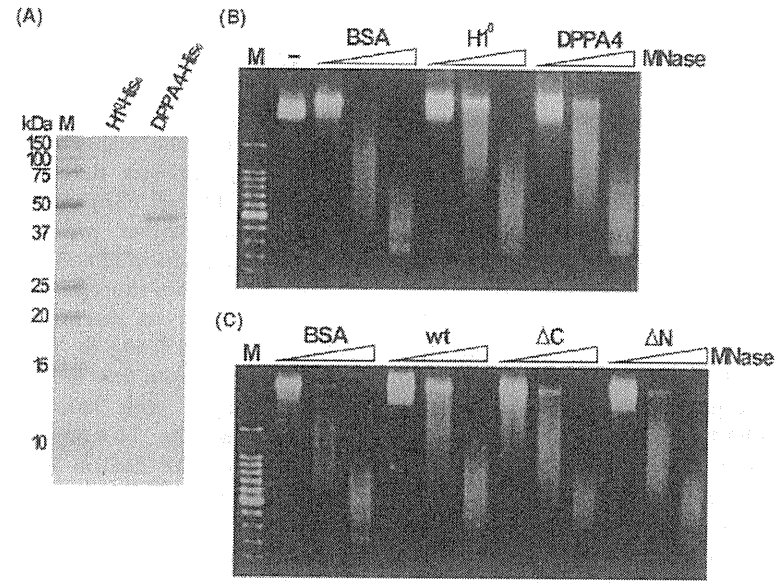

Figure 6 Modulation of chromatin structure by developmental pluripotency associated 4 (DPPA4). (A) Coomassie brilliant blue staining of the purified recombinant $H1^0$-His_6 and DPPA4-His_6 proteins from *E. coli*. M, molecular mass markers. (B) *In vitro* assembled chromatin with BSA, histone $H1^0$-His_6 ($H1^0$), or DPPA4-His_6 (DPPA4) was digested with increasing amount of MNase. (C) *In vitro* assembled chromatin with BSA, DPPA4-His_6 (wt), DPPA4ΔC-His_6 (ΔC), or DPPA4ΔN-His_6 (ΔN) was digested with increasing amount of MNase. Marker (M), 100-bp ladder.

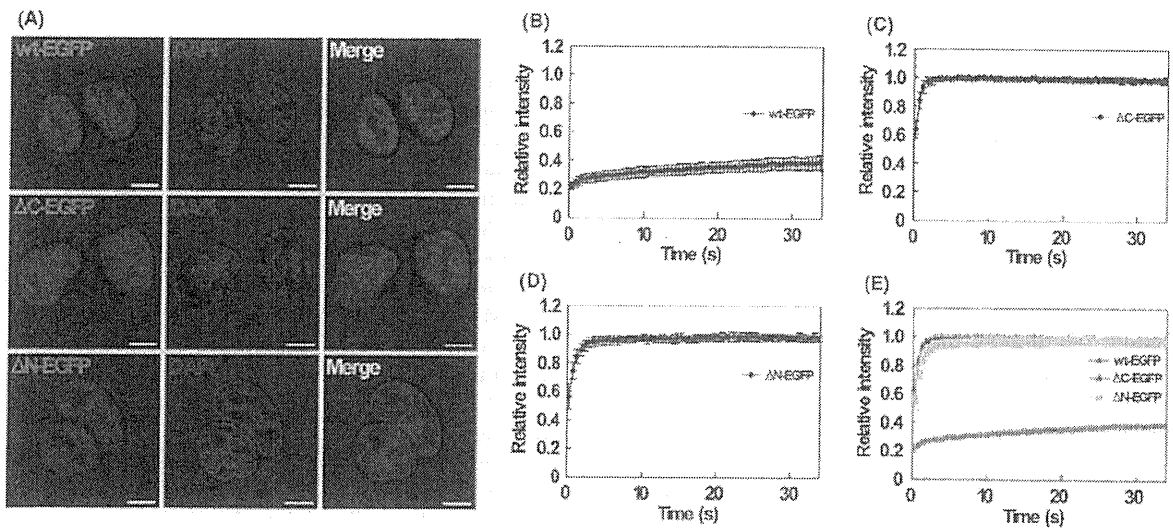

Figure 7 Cellular localization and fluorescence recovery after photobleaching (FRAP) analysis of truncated developmental pluripotency associated 4 (DPPA4) proteins in embryonic stem (ES) cells. (A) Confocal images of ES cells, showing fluorescent DPPA4-EGFP, DPPA4ΔC-EGFP, and DPPA4ΔN-EGFP (green). Nuclei were counterstained with DAPI (blue). Scale bars, 5 μm. (B–D) Quantitative FRAP analysis (FRAP recovery curves) in ES cells transiently expressing wt DPPA4-EGFP (B), DPPA4ΔC-EGFP (C), and DPPA4ΔN-EGFP (D). Each value is the mean ± SD. (E) Comparison of FRAP recovery curves between ES cells expressing DPPA4 wt-EGFP (red), DPPA4ΔC-EGFP (green), and DPPA4ΔN-EGFP (yellow).

to both DNA and histone H3 is required for the proper dynamics in ES cell chromatin.

Discussion

Some FRAP studies concerning ES cells have previously been reported: Meshorer *et al.* (2006) showed that architectural chromatin proteins such as linker histone H1 and heterochromatin protein 1 (HP1) loosely bind to chromatin; and van den Boom *et al.* (2007) revealed that undifferentiated embryonic cell transcription factor 1 (UTF1) is a strong chromatin-associated protein with a dynamic mobility similar to core histones. In the present study, we showed that the mobility of DPPA4 is different from that of core histones and similar to that of linker histone H1 in ES cells (Fig. 2). Previous studies have shown that histone H1 moves slowly compared with other chromatin binding factors such as HP1 and high-mobility-group (HMG) proteins (Phair *et al.* 2004), indicating that DPPA4, like histone H1, is a slow-moving mobile protein binding to chromatin. In addition, histone H1 is not a major global regulator of transcription, although histone H1 maintains the chromatin structure (Fan *et al.* 2005). Thus, it is predicted that DPPA4 is mainly involved in the maintenance of the genome-wide chromatin structure rather than overall transcriptional regulation, like histone H1. We also showed that the addition of DPPA4 enhances the resistance to MNase digestion (Fig. 6). It has been reported that histone H1 and poly(ADP-ribose) polymerase-1 (PARP-1) exert a similar effect on reconstituted chromatin as modulator of chromatin structure (Kim *et al.* 2004). Thus, it is likely that DPPA4 modulates the chromatin structure like histone H1 and PARP-1. Furthermore, DPPA4 is associated with DNA and core histone H3 (Figs 3 and 4), and it could not bind to histone H1 in our immunoprecipitation conditions (data not shown). Based on these results, we propose that DPPA4 modulates the chromatin structure via association with histone H3 and DNA in ES cells. We previously reported that DPPA4 plays an important role in the maintenance of pluripotency in association with active chromatin in ES cells (Masaki *et al.* 2007). Recently, it was suggested that the chromatin states of many inactive genes (so-called bivalent domains) are more permissive for transcription in ES cells than in differentiated cells (Spivakov & Fisher 2007). Taken together, DPPA4 is likely to contribute to the maintenance of these unique chromatin states in ES cells by modulating the chromatin structure in the permissive bivalent domain into a compact state. It has recently been reported that DPPA4 interacts with ES cell chromatin-remodeling complex es-BAF (Brg/Brahma-associated factors) required for pluripotency in ES cells (Ho *et al.* 2009). In addition, the chromatin-remodeling factor Chd1 required for pluripotency regulates the unique open chromatin structure of ES cell (Gaspar-Maia *et al.* 2009). These reports raise another possibility that DPPA4 is involved in chromatin remodeling and maintenance of the open chromatin structure in ES cells. Further studies are necessary to determine whether DPPA4 is involved in modulating the chromatin structure into the compact or open state in ES cells.

The analysis with truncated DPPA4 proteins revealed that the N-terminal region of DPPA4 including the SAP domain has an affinity to DNA, whereas the C-terminal region has a higher affinity to histone H3 than the N-terminal region (Fig. 5). Dppa2/4 conserved region included in the C-terminal region of DPPA4 (Siegel *et al.* 2009) seems to play an important role in association with histone H3. Both truncated DPPA4 proteins showed a weak effect on resistance to MNase digestion compared with wt DPPA4 (Fig. 6), allowing us to consider a possibility that the N-terminal and C-terminal regions of DPPA4 coordinately contribute to the proper formation of chromatin structure. In addition, N-terminal and C-terminal regions are essential for the proper mobility of DPPA4 in ES cells (Fig. 7). These analyses with truncated proteins support our model that DPPA4 modulates the chromatin structure in association with DNA and histone H3.

In our previous report, we suggested that DPPA4 associated with active chromatin contributes to the maintenance of pluripotency in ES cells without feeder cells (Masaki *et al.* 2007). However, it has been recently reported that DPPA4-deficient ES cells normally proliferate in the undifferentiated state on feeder cells (Madan *et al.* 2009). It is difficult to explain rationally the difference between our and their reports; there might be a difference between knockdown of DPPA4 expression and knockout of the gene, or a difference in culture conditions. Alternatively, DPPA4-deficient ES cells are more likely to lead to differentiation. However, the underlying common question is the actual role of DPPA4 in ES cells. In the present study, we investigated the behavior of DPPA4 focusing on the biochemical function of DPPA4 as a chromatin factor, and showed that DPPA4 has a similar mobility to linker histone H1, and directly interacts with DNA and histone H3 via the N- and C-terminal regions, respectively. Moreover, the chromatin